Title: Oncogenic protein condensates modulate cell signal perception and drug tolerance.

Authors: David Gonzalez-Martinez[1#], Lee Roth[1#], Thomas R. Mumford[1], Asmin Tulpule[2], Trever G. Bivona[3], Lukasz J. Bugaj[1,4,5,*]

Affiliations:
[1]Department of Bioengineering, University of Pennsylvania, Philadelphia, PA, 19104, USA
[2]Division of Pediatric Hematology/Oncology, UCSF, San Francisco, CA 94143, USA
[3]Department of Medicine, Division of Hematology and Oncology, UCSF, San Francisco, CA 94143, USA
[4]Abramson Cancer Center, University of Pennsylvania, Philadelphia, PA, 19104, USA
[5]Institute of Regenerative Medicine, University of Pennsylvania, Philadelphia, PA, 19104, USA

[#]equal contributions
[*]corresponding author

Correspondence: bugaj@seas.upenn.edu

Abstract
Drug resistance remains a central challenge towards durable cancer therapy, including for cancers driven by the EML4-ALK oncogene. EML4-ALK and related fusion oncogenes form cytoplasmic protein condensates that transmit oncogenic signals through the Ras/Erk pathway. However, whether such condensates play a role in drug response or resistance development is unclear. Here, we applied optogenetic functional profiling to examine how EML4-ALK condensates impact signal transmission through transmembrane receptor tyrosine kinases (RTKs), a common route of resistance signaling. We found that condensates dramatically suppress signaling through activated RTKs including EGFR. Conversely, ALK inhibition restored and hypersensitized RTK signals. Modulation of RTK sensitivity occurred because EML4-ALK condensates sequestered downstream adapters that are required to transduce signals from both EML4-ALK and ligand-stimulated RTKs. Strikingly, EGFR hypersensitization resulted in rapid and pulsatile Erk signal reactivation within 10s of minutes of drug addition. EGFR reactivation originated from paracrine signals from neighboring apoptotic cells, and reactivation could be blocked by inhibition of either EGFR or matrix metalloproteases. Paracrine signals promoted survival during ALK inhibition, and blockade of paracrine signals accelerated cell killing and suppressed drug tolerance. Our results uncover a regulatory role for protein condensates in cancer signaling and drug response and demonstrate the potential of optogenetic profiling for drug discovery based on functional biomarkers in cancer cells.

Introduction

Despite the development of potent oncogene inhibitors, drug resistance remains an unsolved challenge towards durable cancer therapies. Thus, there remains a critical need to better understand molecular interactions between host cells, oncogenes, and targeted inhibitors to identify effective treatment strategies that forestall or prevent resistance.

The oncoprotein EML4-ALK (echinoderm microtubule-associated protein-like 4-anaplastic lymphoma kinase) is a receptor tyrosine kinase (RTK) fusion oncogene that drives ~3-7% of non-small cell lung cancer (NSCLC), the leading cause of cancer-related death in the US (Takeuchi et al. 2012;

46 Siegel et al. 2021). RTK fusions are a large class of chimeric oncogenes that share a similar
47 composition, where the enzymatic fragment of an RTK is fused through chromosomal rearrangement to
48 a fusion partner domain that is often multimeric (Shaw et al. 2013; Du and Lovly 2018). Cancers driven
49 by RTK fusions commonly exhibit oncogene addiction, where blockade of the oncogene causes cell
50 death(Weinstein 2002). For EML4-ALK+ cancers, multiple FDA-approved ALK inhibitors achieve initial
51 patient responses and tumor regression, although resistance and tumor relapse inevitably emerge
52 (Gainor et al. 2016; Solomon et al. 2018).
53 EML4-ALK drives oncogenicity primarily through sustained Ras/Erk signaling (Hrustanovic et al.
54 2015). Durable treatment of cancers driven by Ras/Erk has been challenged by robust autoinhibitory
55 feedback loops that result in pathway reactivation after treatment. For example, in the case of BRAF
56 V600E+ cancers, BRAF inhibition leads to relief of negative feedback loops that permit strong EGFR
57 stimulation, cell survival, and drug resistance (Lito et al. 2012a; Prahallad et al. 2012a; Gerosa et al.
58 2020a; Corcoran et al. 2012). For EML4-ALK+ cancers, re-activation of RTK signals after ALK inhibition
59 also promotes drug tolerance and acquired resistance (Vaishnavi et al. 2017; Sasaki et al. 2011;
60 Hrustanovic et al. 2015; T. R. Wilson et al. 2012; Voena et al. 2013; Tani et al. 2016) (**Figure 1A**),
61 although specific feedback mechanisms that mediate this reactivation are not well understood.
62 Recently it was found that EML4-ALK forms large cytoplasmic protein granules—or
63 condensates— in cancer cells(Hrustanovic et al. 2015; Tulpule et al. 2021) (**Figure 1B**). Condensate
64 formation resulted in part from the ability of RTK adapter proteins like Grb2 to enlarge small EML4-ALK
65 oligomers through multivalent interactions. Such higher-order assemblies of proteins may have
66 numerous and even opposing consequences on intracellular biochemistry, for example acting as
67 amplifiers or inhibitors of molecular reactions(Banani et al. 2017). Although condensate formation
68 serves as an amplifier that promotes EML4-ALK activation and signaling, it is unclear whether
69 condensates might have additional impact on a cell's ability to transmit signals. Of particular interest are
70 functional interactions between EML4-ALK condensates and transmembrane RTKs including the
71 epidermal growth factor receptor (EGFR), which signal through the same downstream effectors as
72 EML4-ALK (**Figure 1C)**. These interactions are potentially important because EGFR is overexpressed
73 in over 80% of NSCLC and is correlated with poor prognosis (Rusch et al. 1993) and drug resistance
74 (Vaishnavi et al. 2017; Tanimoto et al. 2014; T. R. Wilson et al. 2012; Davies et al. 2013; Obenauf et al.
75 2015; Straussman et al. 2012; Lito et al. 2012a).
76 We recently developed a method called 'functional profiling' to detect how oncogene expression
77 alters cell signal transmission (L. J. Bugaj et al. 2018; Lukasz J. Bugaj, O'Donoghue, and Lim 2017). In
78 this approach, we apply precisely defined signaling stimuli, for example using light-activated
79 'optogenetic' signaling probes, and we quantify differential responses in downstream signals,
80 transcription, and cell fate as a function of oncogene expression or drug treatment. Previously,
81 functional profiling revealed that certain BRAF-mutant cancer cells and drug-treated cells exhibited
82 abnormally slow Ras/Erk pathway activation kinetics, and that such kinetics can cause cells to
83 misinterpret dynamic stimuli leading to hyperproliferation(L. J. Bugaj et al. 2018).
84 In the present work, we applied optogenetic profiling to uncover functional relationships between
85 EML4-ALK condensates and transmembrane RTKs (**Figure 1D**). We discovered that EML4-ALK
86 dramatically suppressed RTK signal transmission. We found that suppression resulted not from
87 biochemical feedback, but rather from sequestration of RTK adapters by EML4-ALK condensates.
88 Suppression was rapidly reversed by ALK inhibition, resulting in hypersensitization of RTKs to external
89 growth factors. Restored perception of external ligands promoted rapid EGFR/Erk reactivation after

drug treatment, which suppressed cell killing and permitted tolerance to ALK inhibitors. Our work thus uncovers a signal regulatory role for oncogenic condensates and suggests novel candidate co-targets to enhance the durability of ALK inhibitor therapy.

Results

Optogenetic profiling reveals that RTK signaling is suppressed in EML4-ALK+ cancer cells.

To determine whether EML4-ALK could alter RTK signaling properties, we expressed a light-sensitive fibroblast growth factor receptor (optoFGFR (Kim et al. 2014)) in the STE-1 cancer cell line, which is driven by EML4-ALK(V1) (Lovly et al. 2014) (**Figure 1E, S1A**). We observed signal transmission by applying blue light stimuli and measuring single-cell phospho-Erk (ppErk) levels through immunofluorescence. We found that blue light stimulation of optoFGFR could induce only minimal ppErk signal increase (1.4-fold) above the high basal ppErk levels attributed to active EML4-ALK (**Figure 1F, top)**. We then asked whether signaling responses might change in the presence of ALK inhibition. Pre-treatment with the ALK inhibitor crizotinib (ALKi, 1 μM) eliminated the high tonic ppErk signal observed in untreated cells, consistent with the ability of EML4-ALK to drive strong signals through the Ras/Erk pathway. Strikingly, subsequent light stimulation now drove strong Erk signaling, surpassing levels achieved in the absence of drug (**Fig. 1F, bottom)**. The dynamic range (fold-change) of signal induction increased as a function of light intensity and reached a maximum of 29-fold increase at the highest levels of light stimulation (**Figure 1G**). Notably, ppErk increase in ALKi-treated cells could be measured after stimulation with exceedingly low levels of light (8 mW/cm^2), a level that did not provide measurable increase in untreated cells, suggesting that ALK inhibition can hypersensitize cancer cells to weak RTK signals (**Figure S1B**). We note that although the magnitude of dynamic range increase was dependent on the expression levels of optoFGFR, the general trends described held across all expression levels (**Figure S1C**). These results suggested the existence of a strong negative regulatory interaction between EML4-ALK activity and transmembrane RTK signaling.

EML4-ALK suppresses — and ALK inhibition restores — EGFR signaling

To determine whether negative regulation of RTKs could be observed in the context of native epidermal growth factor receptor (EGFR), we measured ppErk induction upon addition of epidermal growth factor (EGF) in STE-1 and H3122 cells, two EML4-ALK+ cell lines (Lovly et al. 2014) (**Figure 2A)**. Strong (100 ng/mL) EGF stimulation gave minimal ppErk response, but pre-treatment with ALKi resulted in notably increased ppErk dynamic range in both cell lines (1.7- vs 9.5-fold in STE-; 1.7- vs 7.4-fold in H3122) (**Figure 2B,C)**. As before, increased dynamic range was due to lower baseline — but also higher maximal — ppErk signaling, and the magnitude of dynamic range increase was dose-dependent (**Figure 2C, S2A**). Thus, we concluded that EML4-ALK activity suppresses EGFR signaling in cancer cells.

We next asked whether expression of EML4-ALK was sufficient to suppress RTK signaling. We transiently expressed EML4-ALK(V1) in non-transformed lung epithelial Beas2B cells and we observed responses to EGF (**Figure 2D**). As expected, EML4-ALK expression raised basal ppErk levels (t = 0, **Figure 2E**). However, upon addition of EGF, ppErk signaling was weaker (stronger ppErk suppression) than in untransfected cells (**Figure 2E**). Finally, pre-incubation with ALKi reversed suppression of EGFR/Erk signals in transfected cells (**Figure 2E,F**). Collectively, our results show that EML4-ALK expression is sufficient to strongly dampen signaling through transmembrane EGFR, and that ALK inhibition restores and potentiates these signals.

134
135 ***Mapping EGFR suppression using optogenetics***. We sought to understand the molecular
136 mechanism by which EML4-ALK suppressed EGFR signaling. To narrow candidate mechanisms, we
137 first determined the duration of ALKi pre-incubation that was required to observe enhanced EGFR/Erk
138 signaling. We preincubated both STE-1 and H3122 cells with 0-60 min of ALK inhibitor, and we
139 analyzed ppErk levels in response to 15 min of EGF stimulation (**Figure 3A**). In both cell lines, an
140 increase in Erk signal amplitude was observed with as little as 5 min of ALKi pre-incubation (20 minutes
141 total including stimulation), and rose to half-max with only ~15 mins of pre-incubation (**Figure 3B**).
142 Such fast response suggested a primarily post-translational mechanism.
143 To locate the node in the EGFR/Erk pathway that was suppressed by EML4-ALK, we stimulated
144 the pathway at successive nodes using optogenetics in the presence and absence of drug (**Figure**
145 **3C,D**). In addition to optoFGFR, we also generated STE-1 cells that expressed optoSOS, which allows
146 activation of Ras/Erk signals through light-induced membrane recruitment of the SOS catalytic
147 domain(Toettcher, Weiner, and Lim 2013; Benman et al. 2022) (**Figure 3D, S2**). As before, light
148 stimulation of optoFGFR yielded little increase in ppErk, but ppErk induction was enhanced with pre-
149 treatment with ALKi (**Figure 3E, left**), consistent with relief of optoFGFR suppression by ALKi. By
150 contrast, the maximal level of ppErk induced by optoSOS was unchanged by ALKi pre-treatment
151 (**Figure 3E, right**), suggesting that EML4-ALK suppresses signaling upstream of Ras, for example at
152 the receptor level. However, direct immunofluorescence showed that EGF-stimulated phospho-EGFR
153 (pEGFR) levels were unchanged by ALKi pre-incubation (**Figure S3**). Collectively, our results indicate
154 that EML4-ALK suppresses RTK signaling downstream of receptor phosphorylation but upstream of
155 Ras activation, implicating a role for the adapter proteins that couple these two nodes (**Figure 3F**).
156 Oncogene-mediated feedback suppression of RTKs has been described previously, most
157 notably as as a result of Erk-dependent transcriptional and post-translational negative
158 feedback(Prahallad et al. 2012b; Corcoran et al. 2012; Lito et al. 2012b; Gerosa et al. 2020b; Turke et
159 al. 2012). To test the role of Erk-dependent negative feedback in EML4-ALK+ cancer cells, we
160 decoupled ALK inhibition from the loss of Erk signaling using optoSOS stimulation (**Figure 3G**). In this
161 experiment, we again assessed EGF response in STE-1 cells with ALKi preincubation, but we
162 supplemented one experimental group with optogenetic levels of Erk signaling that matched those from
163 drug-naïve STE-1 cells, thus maintaining any Erk-dependent negative feedback that would have been
164 lost through ALK inhibition (**Figure 3 H,I, S4**). Our results showed that ALKi preincubation again
165 increased the strength of EGF induction, and optoSOS stimulation during pre-incubation did not
166 diminish the strength of induction. These results show that in EML4-ALK+ cancer cells, EGFR
167 suppression —and drug-induced relief of suppression — is not mediated by established, Erk-dependent
168 mechanisms (**Figure 3J**).
169
170 ***EML4-ALK condensates suppress EGFR through competitive sequestration of RTK effectors.***
171 We suspected that condensation of EML4-ALK could play a causal role in RTK suppression. To test the
172 effects of such higher-order EML4-ALK organization, we examined EGF response in cells transfected
173 with EML4-ALK mutants that fail to form condensates due to mutations in either the trimerization
174 domain (ΔTD) or the kinase domain (K589M)(Tulpule et al. 2021). In contrast to full-length EML4-ALK
175 (V1) (**Figure 4A, left**), the condensate-deficient mutants had minimal effect EGF-induced Erk activity
176 (**Figure 4A, middle and right**), suggesting that condensation was essential for its ability to modulate
177 EGFR sensitivity.

178 Protein condensation can act as a negative regulator in both natural and engineered systems
179 when it sequesters essential components of biochemical reactions (Thedieck et al. 2013; Omer et al.
180 2018; Garabedian et al. 2021). We thus hypothesized that EML4-ALK condensates suppressed
181 transmembrane RTKs by sequestering the adapter proteins that are required to transmit RTK signals.
182 Such adapters, including Grb2 and SOS1 which link RTKs to Ras/Erk signaling, are also required to
183 transmit EML4-ALK signals (Tulpule et al. 2021), and thus represent shared resources that could
184 implement competitive inhibition of RTKs.
185 To test this hypothesis, we observed the localization of the Grb2 adapter using Beas2B cells where
186 Grb2 was fluorescently tagged at the endogenous locus (Tulpule et al. 2021). In normal cells, Grb2
187 appeared diffuse in the cytoplasm but translocated to activated EGFR within <1 min of EGF addition
188 (**Fig. 4D,E, Supplementary Movie 1)**. However, upon transfection with EML4-ALK, Grb2 strongly
189 colocalized with EML4-ALK puncta (**Figure S5**), and Grb2 remained sequestered in the puncta even
190 upon addition of EGF (**Figure 4D,E,F, Supplementary Movie 1**). We then asked how Grb2 localization
191 might change in the presence of ALKi (**Figure 4G**). ALKi caused Grb2 puncta to rapidly dissolve into
192 the cytoplasm ($t_{1/2}$ = 17 +/- 2 min) (**Figure 4H,I, Supplementary Movie 2**), in line with recent reports
193 (Sampson et al. 2021). Finally, sequential treatment with ALKi and EGF allowed robust membrane
194 translocation of Grb2 even in the presence of EML4-ALK (**Figure 4J,K**). These results suggest that
195 EML4-ALK condensates sequester Grb2 and suppress translocation to the membrane upon EGF
196 stimulation, providing a mechanism by which EML4-ALK can competitively inhibit EGFR signaling.
197 As a further test of our model, we measured the EGF-induced recruitment of SOS1 in H3122
198 cancer cells through co-immunoprecipitation. SOS1 is recruited by Grb2 to activated receptors and
199 stimulates Ras upon recruitment. We found that SOS1 co-precipitated with EGFR upon EGF
200 stimulation, but only when preincubated with ALKi, further suggesting that active EML4-ALK
201 condensates sequester RTK adapters (**Figure 4J, S6**). Finally, our conceptual model predicts that
202 distinct RTK fusions that form condensates would similarly repress EGFR signaling. We thus measured
203 EGF response in TPC-1 cells, which harbor the CCDC6-RET fusion. Like EML4-ALK, CCDC6-RET
204 forms condensates that colocalize with many RTK adapters, including Grb2 and SOS1(Tulpule et al.
205 2021). As predicted, EGF stimulation induced only moderate levels of Erk phosphorylation, whereas
206 pre-treatment with RET inhibitor BLU-667 permitted strong stimulation (2.2- vs 7-fold stimulation) to
207 levels beyond those achievable in drug-naive cells (**Figure S7**). Collectively, our results suggest that
208 competition for RTK adapters is a key mechanism by which condensates of EML4-ALK —and
209 potentially other RTK fusions — suppress a cell's perception of transmembrane RTK signals (**Fig. 4K**).
210
211 ***RTK resensitization promotes rapid signal reactivation upon ALK inhibition.***
212 RTK stimulation promotes drug tolerance and acquired resistance across cancer types (Straussman et
213 al. 2012; T. R. Wilson et al. 2012). We thus sought to understand whether hypersensitization of RTKs
214 could promote RTK signaling during ALKi therapy. We monitored RTK/Erk signaling in populations of
215 STE-1 cells using ErkKTR, a biosensor that reports on Erk activity through nuclear exclusion of a
216 fluorescent protein (Regot et al. 2014). (**Figure 5A)**. In the absence of ALKi, Erk activity was at an
217 intermediate level, indicated by relatively equal distribution between the cytoplasm and nucleus (**Figure**
218 **5B, Supplementary Movie 3**). Notably, this localization pattern did not change over the course of 22
219 hrs, reflecting the tonic signaling downstream of EML4-ALK. By contrast, treatment with ALKi induced a
220 rapid initial decrease of Erk activity followed by a striking appearance of Erk activity pulses within as
221 little as 30 min after treatment (**Supplementary Movie 3**). Each Erk pulse lasted 10-20 minutes, and

222 the pulse amplitude exceeded levels observed in the absence of drug, paralleling our earlier results
223 with optogenetic or ligand stimulation (**Figure 5C**).
224 Activity pulses appeared sporadically but were not confined to individual cells. Rather, Erk
225 activity appeared in small clusters of neighboring cells either simultaneously or as a wave of activity
226 (**Figure 4B, Supplementary Movie 3**). This pattern was consistent with RTK stimulation through
227 paracrine signaling. To test this hypothesis, we sought to block paracrine signals through inhibition of
228 either the EGF receptor (EGFRi, 1 μM erlotinib) or matrix metalloproteases (MMPi, 10 μM marimastat),
229 which release EGFR ligands from the cell surface to enable paracrine signaling (Dong et al. 1999;
230 Peschon et al. 1998; Sahin et al. 2004). Co-treatment with ALKi and EGFRi suppressed Erk activity
231 pulses after drug addition (ALKi vs ALKi/EGFRi: 58 $\pm$ 7% vs 12 $\pm$ 5% of cells showing $\geq$ 1 pulse over 22
232 hrs; error = 95% CI), indicating EGFR activation causes the observed ERK pulses (**Fig. 4D,E,F,**
233 **Supplementary Movie 3**). Co-treatment with ALKi and MMPi similarly reduced Erk reactivation pulses
234 (ALKi vs ALKi/MMPi: 58 $\pm$ 7% vs 36 $\pm$ 7% of cells showing $\geq$ 1 pulse over 22 hrs; error = 95% CI),
235 though to a lesser extent than with EGFRi, potentially due to MMP-independent juxtacrine signals
236 (Brachmann et al. 1989; Wong et al. 1989) (**Fig. 4D,E,F, Supplementary Movie 3**). Thus, ALKi
237 treatment in STE-1 cells decreases Erk signals but is rapidly followed by RTK reactivation mediated by
238 paracrine signals.
239
240 **Signal reactivation results from paracrine signals from dying cells.**
241 We next sought to determine the source of the paracrine signals. We observed that pulsing
242 events often appeared next to dying cells, and that co-inhibition of ALKi with EGFRi or MMPi prevented
243 this pulsing (**Figure 5G,H, Supplementary Movie 3)**. These observations are consistent with paracrine
244 ligand secretion from apoptotic cells, which has previously been observed to promote cell survival and
245 homeostasis within epithelial sheets (Gagliardi et al. 2021). To quantify this effect, we observed signal
246 activation in cells that neighbored a dying cell within the ~hour preceding cell death (**Figure 5C).** We
247 then counted Erk pulses in these neighbors (N) and compared pulse counts to those from randomly
248 selected non-neighbors (R) over that same time interval (for more details, see **Methods).** Our analysis
249 revealed that, in the absence of ALKi, pulses were almost never observed in either the N or R
250 populations (DMSO, **Figure 5 D,E**). However, in ALKi-treated cells, N cells pulsed significantly more
251 than R cells (N vs R: 27 $\pm$ 4% vs 4 $\pm$ 2% cells with $\geq$ 1 pulse; error = 95% CI) (**Fig. 5D,E)**. Co-treatment
252 with EGFRi eliminated Erk pulsing in neighbors (N cells in ALKi vs ALKi/EGFRi: 27 $\pm$ 4% vs 2 $\pm$ 1%),
253 whereas co-treatment with MMPi dramatically reduced neighbor signaling relative to ALKi alone (N cells
254 in ALKi vs ALKi/MMPi: 27 $\pm$ 4% vs 10 $\pm$ 2%),(**Fig. 5D,E).** Together, our results demonstrate that
255 virtually all observed Erk reactivation is associated with paracrine signals associated with dying drug-
256 treated cells. Importantly, because Erk pulses were not observed in untreated cells —even in neighbors
257 of dying cells (**Figure 5J**)—these data suggest that ALKi-induced RTK hypersensitization is an
258 essential first step for the perception of paracrine ligands during ALKi therapy.
259
260 ***Signal reactivation pulses activate gene transcription***
261 To understand the extent to which the short ALKi-dependent Erk pulses could impact cell
262 behavior, we asked whether the observed pulses could stimulate downstream transcription. Erk activity
263 is a strong driver of transcription, including of a class of rapidly responding immediate early genes
264 (IEGs) that begin transcription within minutes of Erk activity(M. Z. Wilson et al. 2017). EGR1 is an IEG
265 that has been implicated in drug resistance to ALK inhibitors (Voena et al. 2013). Additionally, EGR1

expression is adaptive, such that its expression peaks by ~ 1 hr but then decays within 1-2 hours, even in the presence of constant upstream signal (Sukhatme et al. 1987) (**Figure S8A**). Thus, accumulation of EGR1 indicates the presence of only recent Erk activation. We thus examined the extent to which EGR1 accumulated in STE-1 cells upon drug treatment (**Fig. 6A**). In untreated cancer cells, EGR1 levels remained low despite high Erk signaling from EML4-ALK, consistent with EGR1 adaptation to tonic Erk signals (**Figure 6B,C)**. Upon ALK inhibition, a distinct peak of EGR1-high cells appeared and grew at 4 and 6 hrs after drug treatment, indicating that ALKi-induced Erk pulses could indeed drive transcription. Importantly, co-inhibition of ALK and EGFR prevented the appearance of EGR1-positive cells, consistent with transcription resulting from paracrine signals through EGFR (**Figure 6B,C)**. Thus, ALKi-induced Erk activity pulses provide sufficient signal to drive gene expression changes that could regulate cell fate.

Signal reactivation promotes acute drug tolerance and cell persistence during ALK inhibition. Finally, we asked whether RTK hypersensitization and resultant Erk activity pulses could counteract cell killing and promote drug tolerance to ALK inhibitor therapy (**Fig. 6D).** In STE-1 cells imaged over 22 hrs, ALKi treatment induced moderate cell death (45 $\pm$ 7% of cells; error = 95% CI). However, co-treatment of ALKi with either EGFRi or MMPi increased cell death (52 $\pm$ 7% and 75 $\pm$ 6% of cells, respectively) (**Fig. 6E)**. In both ALKi- and ALKi/MMPi-treated cells, surviving cells showed an increased number of Erk pulses compared to cells that died (ALKi, live vs dead: 1.8 $\pm$ 0.2 vs 0.9 $\pm$ 0.1 pulses per cell; ALKi/MMPi, live vs dead: 1.6 $\pm$ 0.2 vs 0.4 $\pm$ 0.1 pulses per cell. Mean $\pm$ SE, **Figure 6F**), further drawing a link between RTK reactivation and cell survival. We confirmed our results through an independent assay of cell death using a fluorescent reporter of caspase-3 activity (Nucview), an indicator of apoptosis, over the first 24 hr of treatment in EML4-ALK+ cells. As before, while ALK inhibition led to increased caspase-3, co-treatment with EGFRi significantly increased the caspase-3+ cell fraction in STE-1 cells (28 ± 2 vs. 41 ± 2%). Similarly, co-treatment with MMPi also increased caspase-3 (from 28 ± 2 to 50 ± 6%) (**Figure 6G**). Similar trends were observed in H3122 cells (**Figure S8B).** Neither EGFRi nor MMPi treatment alone showed enhanced killing over untreated cells. Notably, addition of 50 ng/mL EGF reversed enhanced killing in the ALKi/MMPi condition in STE-1 cells (61 ± 2 to 39 ± 1%, respectively), further suggesting that synergistic killing in the presence of MMPi resulted from blockade of signal reactivation (**Figure 6H**). Although EGF addition could not rescue enhanced killing under combined ALKi/EGFRi treatment, optogenetic pulses of optoFGFR lowered cell death in this condition (**Figure S8C,D,E**). Finally, we observed that co-treatments of ALKi with either EGFRi or MMPi dramatically suppressed long-term drug tolerance measured at 17-days (**Figure 6I**). Together, our results indicate that hypersensitization of EGFR and restored perception of paracrine ligands leads to reactivation of survival signals soon after drug treatment, which limits the cytotoxicity of ALK therapies and promotes drug tolerance, the first step towards acquired resistance. The mechanisms that underlie these events may thus provide novel treatment co-targets for to enhance therapy in EML4-ALK+ cancers.

Discussion

Our results advance a novel function for protein condensates in cancer cells and their response to targeted therapy (Jiang et al. 2020). In addition to amplifying oncogenic signaling (Tulpule et al. 2021), EML4-ALK condensates simultaneously act as a molecular sponge for RTK adapters including Grb2 and SOS. This sequestration desensitizes the cell's perception of external ligands by limiting the

amount of adapters available to transduce the activated RTK signal. However, upon ALK inhibition, adapters are rapidly released to the cytoplasm, hypersensitizing cellular response to ligands in the cell's microenvironment. RTK hypersensitization promotes cell survival and drug tolerance in response to targeted inhibitors, due at lease in part to apoptosis-induced paracrine signals.

Adapter sequestration by fusion condensates represents a novel mechanism by which oncogenes can suppress RTK signaling. Analogous RTK suppression has been observed in other, molecularly distinct cancers. BRAF V600E+ melanoma and colorectal cancer cells suppress RTKs through Erk-dependent transcription of negative regulators (Sproutys), and through inhibitory phosphorylation of SOS1(Lito et al. 2012b; Prahallad et al. 2012b; Gerosa et al. 2020b). Inhibition of BRAF suppresses these mechanisms and leads to rapid, pulsatile Erk reactivation and drug resistance, similar to our observations. Separately, in cancers driven by EGFR, Erk provides suppressive phosphorylation of EGFR receptors, which is lost during MEK inhibition and leads to reactivation of ErbB3 and PI3K(Turke et al. 2012). In contrast to these and similar examples, our findings demonstrate that such RTK suppression can also be implemented through biophysical, rather than biochemical, feedback. Nevertheless, the variety of mechanisms by which oncogenes can suppress RTKs hints that such feedback might play an important role in establishing permissive conditions for oncogenesis. It will thus be interesting to more comprehensively understand the diverse oncogenic contexts in which such suppression and reactivation occurs.

It has been repeatedly observed that ligand-induced signaling through EGFR promotes survival and resistance to ALK inhibitors in EML4-ALK+ cancer cells (T. R. Wilson et al. 2012; Vander Velde et al. 2020; Tani et al. 2016; Tanimoto et al. 2014; Vaishnavi et al. 2017; Sasaki et al. 2011; Obenauf et al. 2015). Our work builds on these prior studies to show that 1) ALK inhibition is a necessary first step to allow cancer cell perception of paracrine signals and 2) ALK-induced resensitization to RTK signals happens within minutes of drug treatment. In addition to fast RTK reactivation, previous work found that slower-timescale transcriptional amplification of KRas or downregulation of DUSP6 contributes to resistance development (Hrustanovic et al. 2015). Our results are complementary to these findings, which could be expected to further sensitize cells to external RTK ligands.

We found that dying cancer cells send survival signals to their neighbors through a mechanism that requires proteolytic processing of EGFR ligands, thus adding to previously identified mechanisms whereby drug treatment induces secretion that promotes cell survival and drug tolerance (Obenauf et al. 2015; Kurtova et al. 2015). Blockade of apoptosis-induced paracrine signals enhanced cell killing and limited tolerance in response to ALK inhibition. Although co-inhibition of EGFR is highly effective in promoting durable drug responses across a variety of cancer cells, (Vaishnavi et al. 2017; Vander Velde et al. 2020; Sasaki et al. 2011; Voena et al. 2013), a recent clinical trial of combined inhibition of crizotinib (ALKi) and erlotinib (EGFRi) in EML4-ALK+ NSCLC failed due to frequent adverse effects and low maximum tolerated dose (Ou et al. 2017). We show that co-inhibition of certain matrix metalloproteases may be an alternative strategy limit RTK signaling during targeted therapy. We note, however, that previous studies found that long-term MMP inhibition can promote resistance by causing accumulation of transmembrane RTKs (e.g. AXL) (Miller et al. 2016). Thus, further studies will be required to understand whether MMPi co-treatment can indeed enhance therapy, or whether MMPi scheduling could leverage acute benefits while avoiding deleterious chronic effects.

Our finding that the sequestration of RTK adapters can functionally desensitize RTK signals could inspire new types of therapeutic targets that mimic this behavior, for example through inhibition or sequestration of important RTK adapters. Of note, the recent discovery of EML4-ALK condensates has

raised the idea that disaggregation of the condensates might be therapeutically beneficial (Hirai et al. 2020; Cai, Liu, and Lippincott-Schwartz 2021). Our work cautions, however, that such disaggregation strategies will likely be subject to the same adapter redistribution and rapid RTK reactivation observed with small molecule ALK inhibitors, potentially challenging their efficacy.

A unique promise of functional profiling is that common signaling abnormalities may be identified and inform therapies among genetically distinct cancers (Lukasz J. Bugaj, O'Donoghue, and Lim 2017). Because our work revealed signaling principles that result from a likely common property (condensation) of RTK fusions (Du and Lovly 2018; Tulpule et al. 2021), we anticipate that our findings may be broadly relevant to other cancer cells in this class. We show that in a cancer line driven by a CCDC6-RET fusion that also forms large aggregates (Tulpule et al. 2021), RET activity similarly suppresses EGFR, and RET inhibition potentiates EGFR signaling (**Figure S7)**. These results are consistent with a previous study that showed that Grb2 can change association from the fusion to EGFR upon kinase inhibition in cancers driven by ALK, RET, NTRK1 and ROS1 fusions, further implying common behavior across molecularly distinct RTK fusions (Vaishnavi et al. 2017). Future work will determine the extent to which the principles we describe in EML4-ALK+ cancers will extend to this more diverse array of malignancies.

Acknowledgements. The authors thank Dr. Magdalena Niewiadomska-Bugaj for feedback on statistics, data presentation and analysis. The authors also thank Dr. Alex Hughes (Penn) and Dr. Sydney Shaffer, and Dr. Yael Mosse for helpful comments on the manuscript. The Beas2B cell line with endogenously tagged Grb2 was a gift from Bo Huang, PhD (UCSF). This work was supported by the National Institutes of Health (R35GM138211 for L.J.B).

Author Contributions D.G.M. and L.J.B. conceived the study. D.G.M. and L.R. performed experiments. D.G.M., T.R.M. and L.J.B. analyzed data. L.J.B. supervised the work. A.T., T.G.B., L.R., and L.J.B. provided experimental feedback and guidance. D.G.M and L.J.B. wrote the manuscript and made figures, with editing from all authors.

Conflicts of interest. D.G.M. and L.J.B. have filed a provisional patent based on the findings in this work.

392 **Figures**

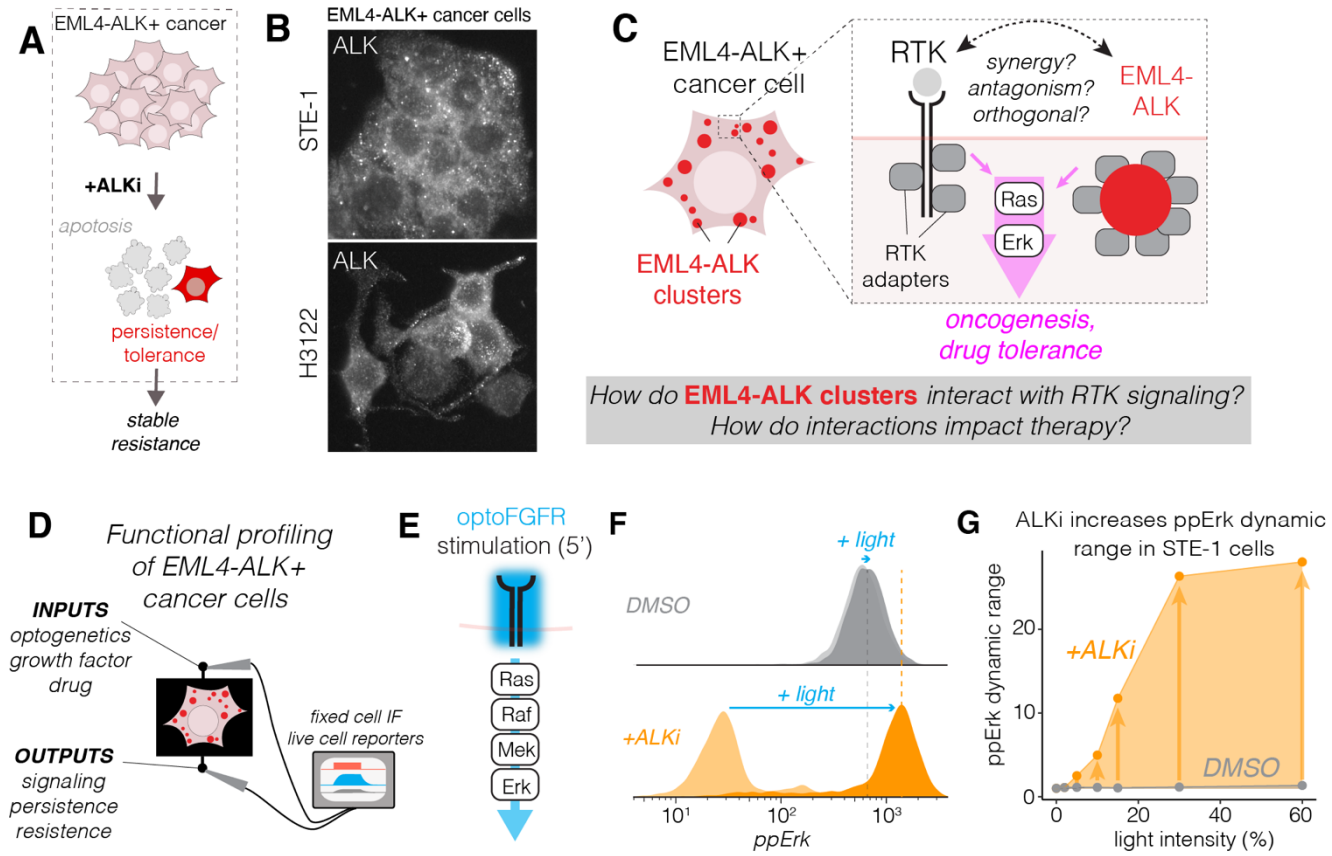

393

394 **Figure 1. Optogenetic functional profiling of EML4-ALK+ cancer cells reveals suppression of**
395 **RTK signaling.** A) EML4-ALK+ cancer cells treated with ALK inhibitors (ALKi) can persist through
396 therapy and acquire stable drug resistance. B) Immunofluorescence staining shows punctate
397 expression of ALK in two EML4-ALK+ cancer cell lines. C) Although EML4-ALK and transmembrane
398 RTKs signal through the same downstream adapters, the extent to which EML4-ALK condensates
399 interact with RTKs, and whether interactions could impact drug responses, is not clear. D) Functional
400 profiling allows us to observe input/output responses to RTK signaling to understand functional
401 interactions between RTKs and EML4-ALK. E) optoFGFR allows blue-light-induced stimulation of
402 FGFR signaling, including through the Ras/Erk pathway. F) Single-cell analysis of ppErk levels in STE-
403 1 cells stimulated with light (optoFGFR) in the presence of either DMSO (grey) or the ALK inhibitor
404 crizotinib (ALKi, 1μM; orange). F) ppErk fold-change in response to 5 min of blue light stimulation. Blue
405 light intensity ranged from 2% to 60% of maximum (1.45 W/cm^2). Data points show the ratio of ppErk
406 from stimulated and unstimulated cells. Each condition was performed in biological replicate, with each
407 replicate representing the mean of ~1000 cells. This experiment is representative of three independent
408 experiments.

409

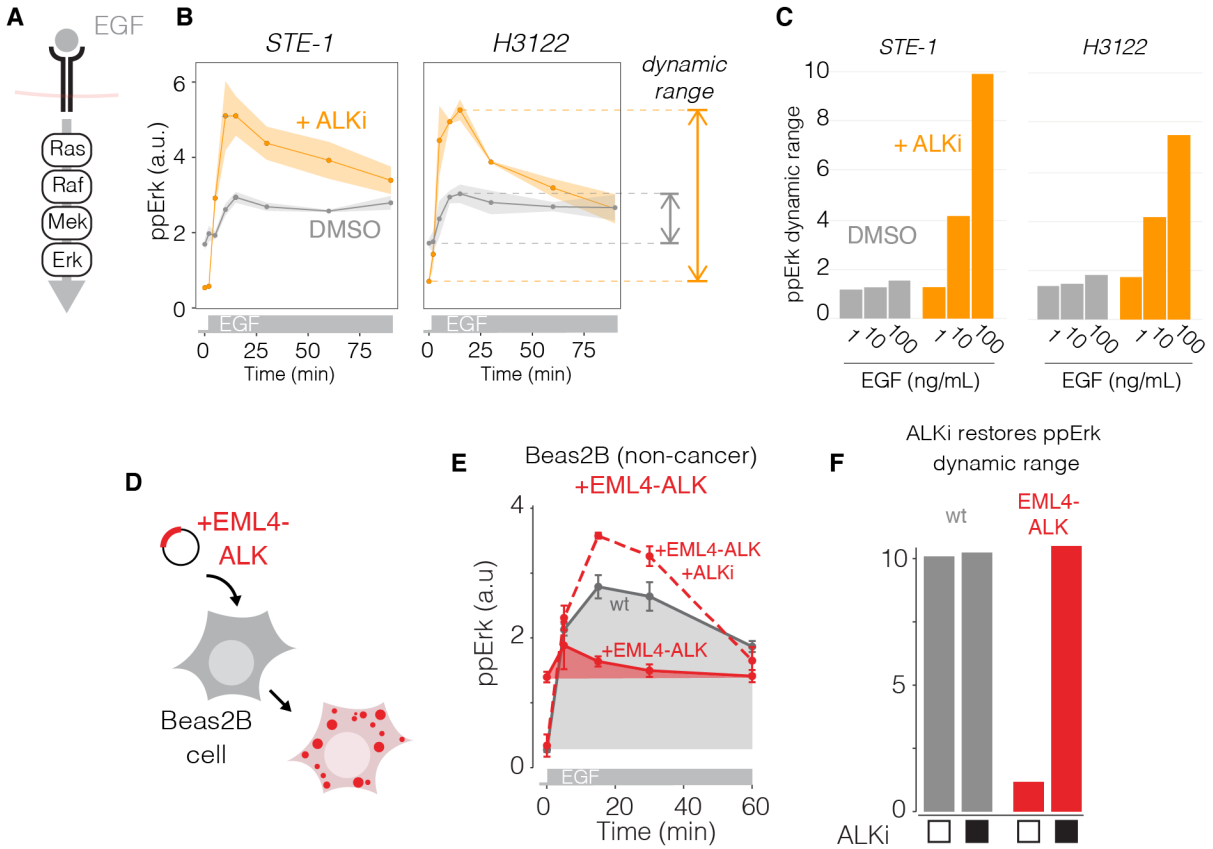

410
411
412
413 **Figure 2. EML4-ALK suppresses EGFR signaling.** A) EGF stimulates EGFR and downstream
414 Ras/Erk signaling. B) ppErk levels in response to EGF (100 ng/mL) in the presence of 1μM ALKi
415 (orange) or DMSO (grey) in STE-1 and H3122 cancer cells. Data points and ribbons represent mean
416 +/- SEM of three replicates, each of which represents the mean of ~1000 cells. C) Quantification of
417 dynamic range from experiment in 2B over a range of EGF concentrations. D) EML4-ALK(V1) was
418 transiently expressed in lung epithelial Beas2B cells. E) Time course of ppErk immunofluorescence
419 levels in response to EGF stimulation (50 ng/mL). Data points represent mean +/- SEM of three
420 replicates. G) Dynamic range of ppErk in EML4-ALK-expressing Beas2B in response to EGF in the
421 presence or absence of ALKi (1 μM) pretreatment.

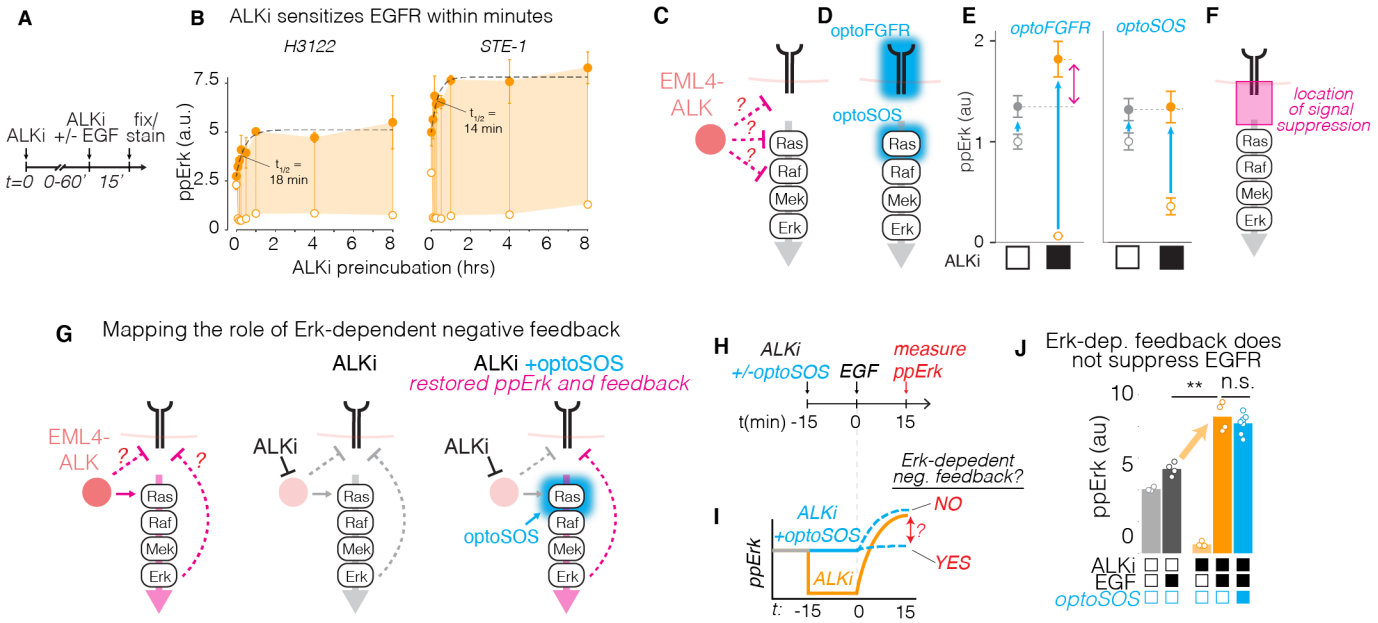

Figure 3. Mapping RTK feedback suppression using optogenetics. A) Time course of RTK hypersensitization was obtained by pre-incubating cancer cells with 1 μM crizotinib for varying times before stimulation with EGF (50 ng/mL) for 15 min, followed by fixation and immunostaining for ppErk. B) ppErk induction as a function of ALKi pre-incubation time, quantified by immunofluorescence. Open circles = unstimulated. Closed circles = EGF stimulated. Data points represent mean +/- SEM of triplicates. Error bars are smaller than the data points for unstimulated samples. C)Pinpointing the location of EML4-ALK interaction with RTK/Erk signaling. D) OptoFGFR and optoSOS permit optogenetic stimulation at successive nodes of the pathway. E) Quantification of immunofluorescence of ppErk in response to optoFGFR or optoSOS in the presence or absence of ALKi. ALK-dependent suppression is observed only with optoFGFR, suggesting that suppression happens upstream of Ras but downstream of RTK activation (F). G) Testing the role of Erk-dependent negative feedback on RTK suppression. Stimulating optoSOS drives high levels of Erk during ALKi treatment and sustains any Erk-dependent negative feedback that would otherwise be lost during ALK inhibition. H) STE-1 cells were treated with either ALKi or ALKi and optoSOS, and EGF response was assessed. I) Predicted results and implications for Erk-dependent feedback. J) Cells treated with both ALKi and optoSOS showed the same increase in EGF-induced ppErk as cells receiving ALKi only, suggesting that Erk-dependent negative feedback does not suppress EGFR in EML4-ALK+ cancer cells. Data points represent means of ~600-1000 cells per condition.

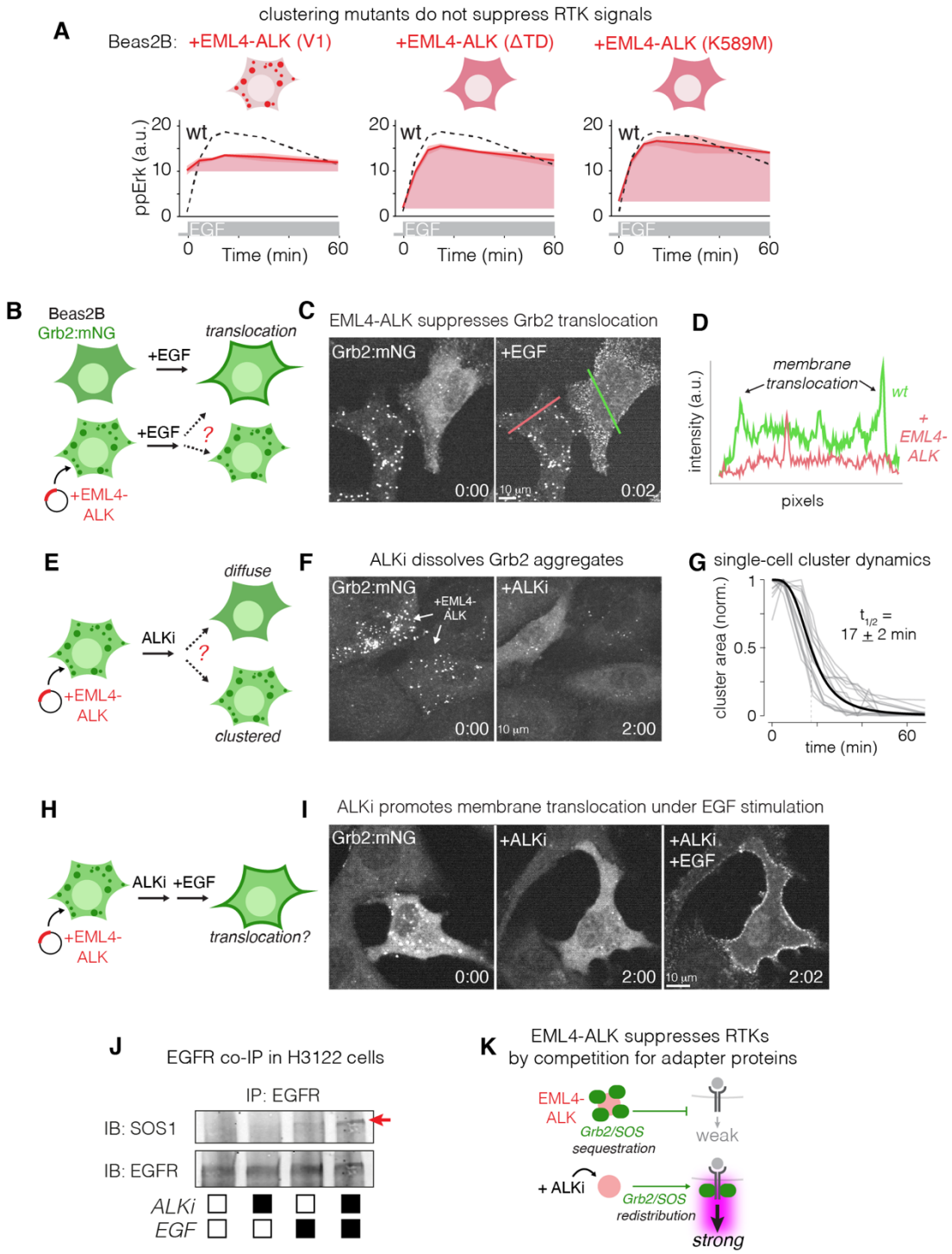

Figure 4. EML4-ALK condensates suppress RTK signals through sequestration of RTK effectors. A) Quantification of ppErk response to EGF (50ng/mL) stimulation in Beas2B cells that expressed EML4-ALK (V1), EML4-ALK (ΔTD), and kinase-dead EML4-ALK (K589M). Data are means of biological triplicates, each of which represents the mean of 500-1000 cells. Error = 1 SEM. B) Beas2B cells that harbored endogenously-tagged Grb2 (Grb2:mNG) were transiently transfected with EML4-ALK and stimulated with EGF (50ng/mL) to visualize Grb2 translocation in the presence and absence of EML4-ALK. C) Impaired membrane translocation of Grb2 in the presence of EML4-ALK

condensates. Time in mm:sec. See Supplementary Movie 1. D) Line scan of Grb2 intensity distribution in the presence (red) or absence (green) of EML4-ALK expression, as depicted in C. E) Grb2 localization was visualized upon treatment with 1 μM ALKi. F) Grb2 shifted from condensates to cytoplasm after ALKi treatment. Time in hh:mm. See Supplementary Movie 2. G) Quantification of Grb2 cluster dissociation kinetics after ALKi treatment. H) Grb2 distribution was examined upon sequential treatment with ALKi and EGF. I) ALKi released Grb2 to the cytoplasm, which allowed its membrane translocation in the presence of EGF. J) Immunoprecipitation of EGFR shows co-precipitation of SOS1 only in the presence of ALKi pretreatment and EGF. K) EML4-ALK sequesters adapters like Grb2/SOS1 and prohibits their translocation to RTKs upon ligand stimulation. ALK inhibition releases adapter sequestration and restores cellular response to RTK stimulation.

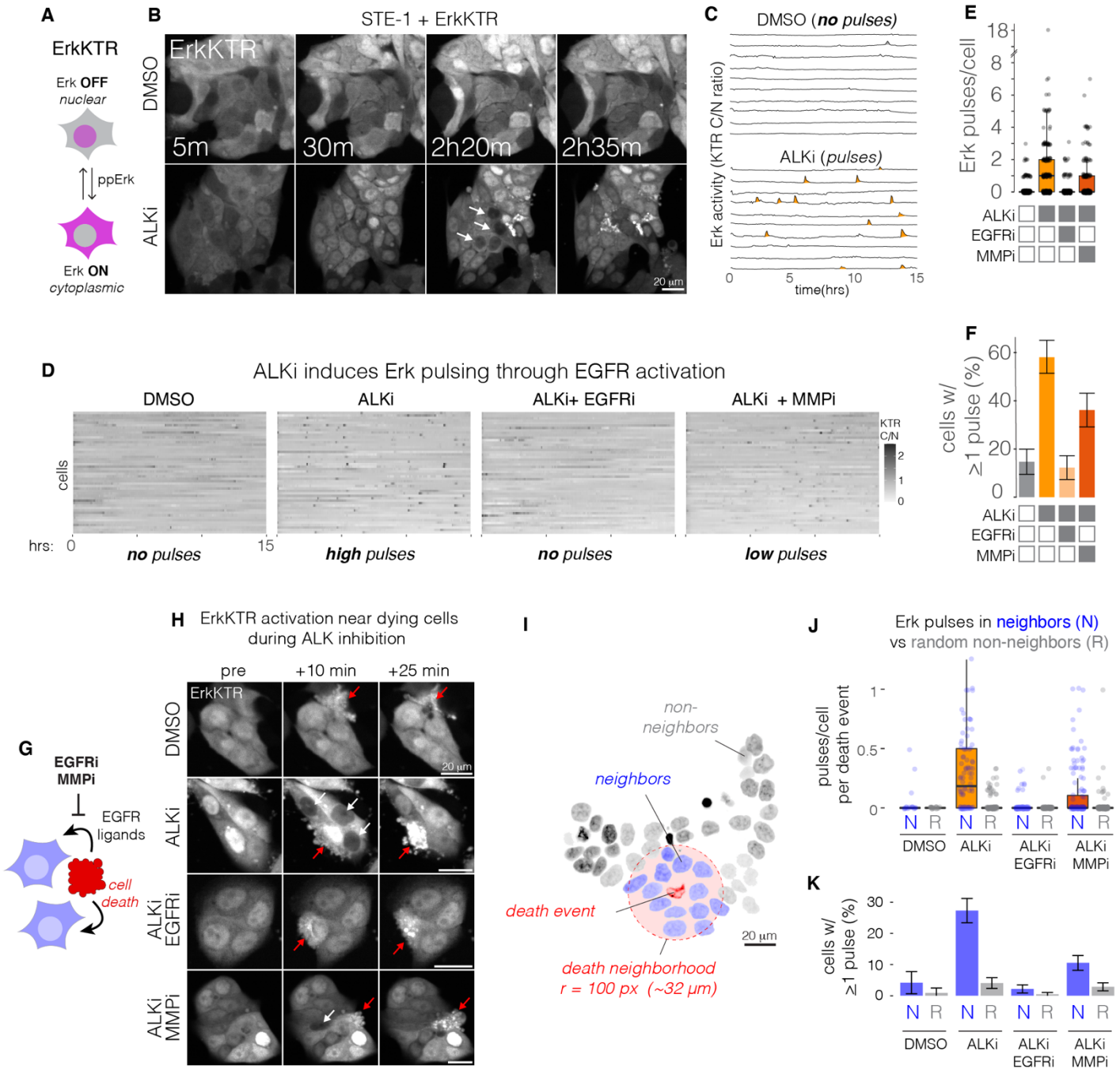

Figure 5. ALK inhibition resensitizes cancer cells to paracrine growth factors secreted from dying neighbor cells. A) The ErkKTR reporter indicates Erk activity through nuclear-cytoplasmic translocation of a fluorescent protein. (B) Live cell imaging of STE-1 cells expressing ErkKTR in the presence or absence of ALKi (1 µM crizotinib). See **Supplementary Movie 3**. C) Representative single-cell traces of cytoplasmic/nuclear ErkKTR intensity ratio from conditions shown in B. D) Quantification of ErkKTR activity in the presence of ALKi or its combination with EGFRi (1 µM erlotinib) or MMPi (10 µM marimastat). E) Quantification of Erk activity pulses per cell. F) Fraction of cells that exhibited any pulses over 21.5 hrs of imaging. Error bars indicate 95% CI. n = 200 cells per condition.

G) Apoptotic cells can secrete paracrine EGFR ligands to their neighbors. Paracrine signaling can be blocked by inhibiting either EGFR or the MMPs that are required to shed certain EGFR ligands from the surface of the sender cell. H) ErkKTR activity pulses are primarily observed surrounding a dying cell during ALK inhibition, but not in the absence of drug or in the presence of EGFR or MMP inhibitors. I) Definition of neighbors and non-neighbors of a death event. J) Quantification of pulses per cell for each death event in neighbors or a randomly-chosen subset of cells not near a death event (see **Methods** for more details). K) Fraction of total neighbor vs random non-neighbor cells that show any pulsing. Error bars = 95% CI.

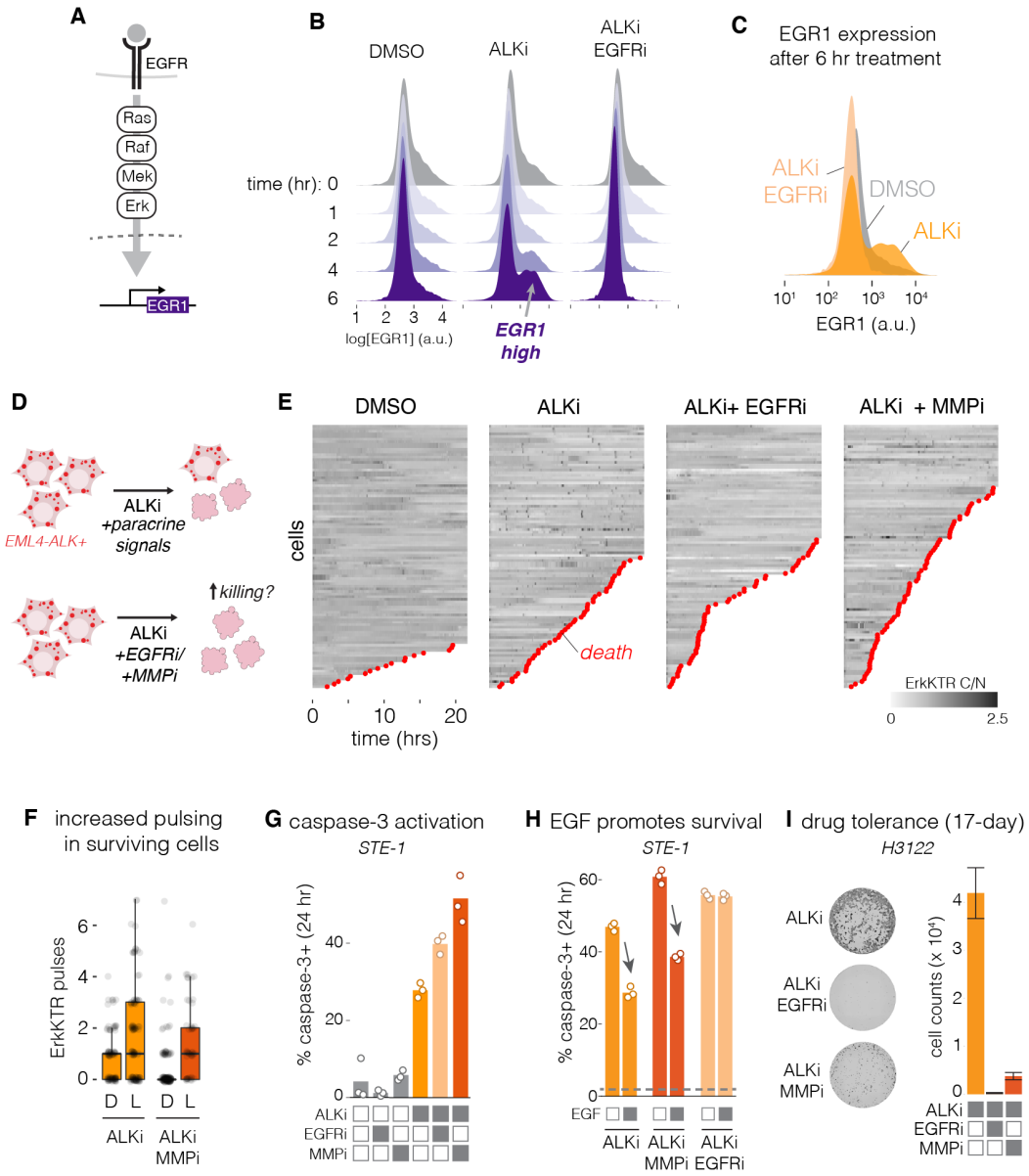

FIgure 6. Resensitization to paracrine signals drives transcription and promotes drug tolerance. A) Signaling through EGFR activates Ras/Erk and stimulates transcription, including of the immediate early gene EGR1. B) Upon ALK inhibition, EGR1 expression increases, but not upon co-inhibition of ALK and EGFR. C) Comparison of EGR1 expression after 6 hrs of the indicated treatment. D) We hypothesized that restored perception of paracrine signals might promote survival, and that blocking paracrine signals would promote killing. E) Visualization of live cell imaging of Erk activity pulses and cell death. F) Quantification of pulse per cell in cells that died (D) or survived (L) through 22 hrs of imaging, in the conditions where Erk pulsing could be observed. H) Caspase-3 activation was assessed using the NucView reporter after 24 hr treatment with the indicated drugs. I) EGF (50 ng/mL) addition promotes survival during ALKi treatment and counteracts enhanced killing from ALKi/MMPi co-treatment, but not from ALKi/EGFRi co-treatment. Dotted line is cell killing from DMSO control treatment. Each data point represents the fraction of caspase-3+ cells out of ~10,000 total cells. See **Methods** for more details. I) Crystal violet staining (left) and cell counts (right) of cell survival after 17 days of the indicated treatments.

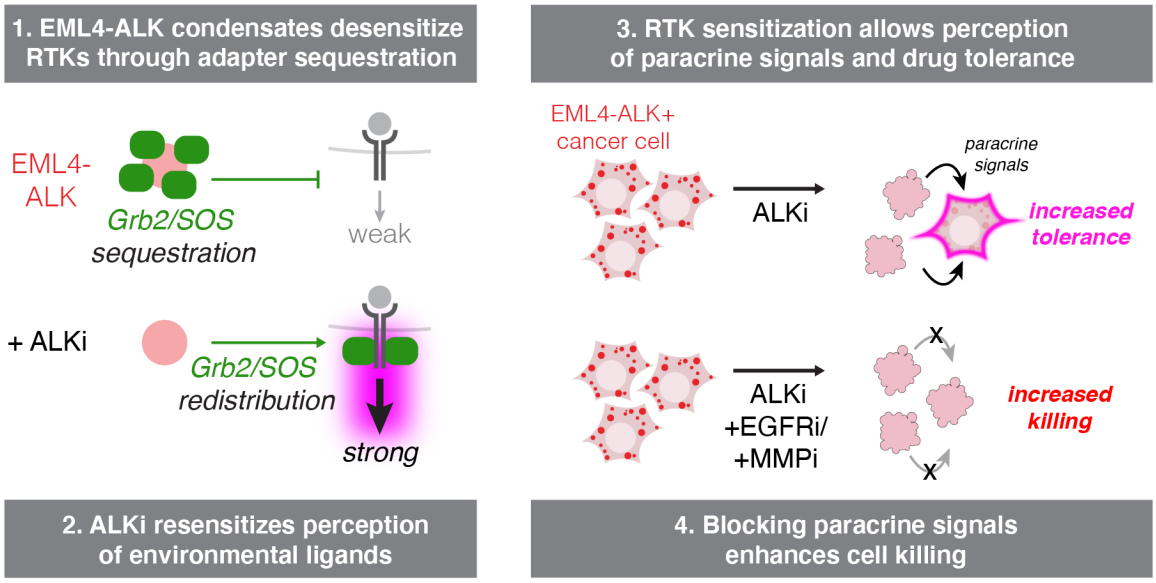

Figure 7. Model of how EML4-ALK condensates interact with transmembrane RTKs and its effect on drug tolerance. We find that EML4-ALK condensates suppress perception of EGFR signals by sequestering RTK adapters like Grb2 and SOS1. Upon ALK inhibition, adapters are released to the cytoplasm where they can transduce signals from EGFR and other RTKs. Although ALK inhibitors effectively suppress ALK activity, they simultaneously restore a cell's perception to paracrine signals, including those from neighboring apoptotic cells. Such paracrine signals promote drug tolerance, and blocking them with inhibitors of either EGFR or MMPs enhances cell killing during ALK inhibitor therapy.

Supplementary Figures

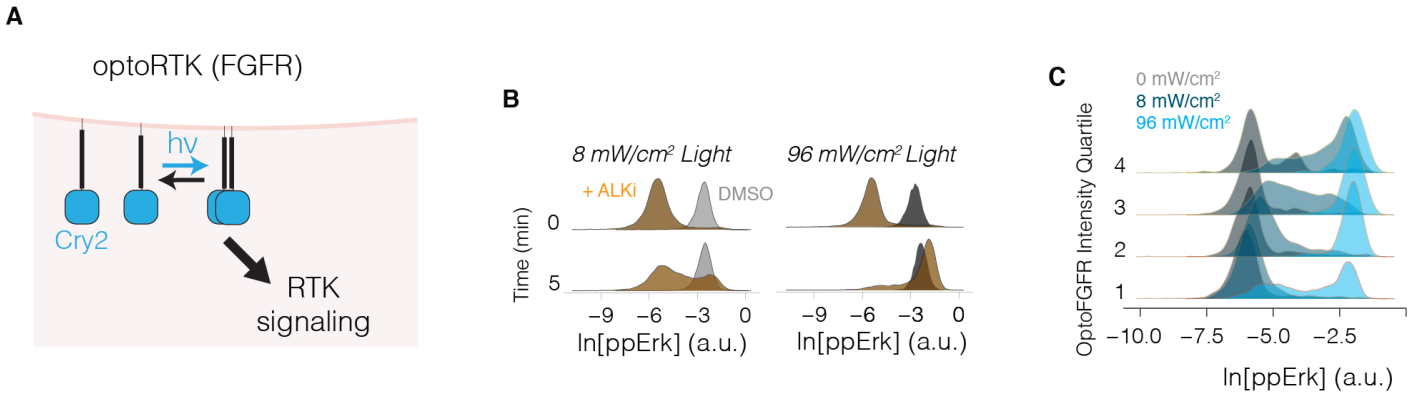

Supplementary Figure 1. OptoFGFR functional profiling of STE-1 cancer cells. A) optoFGFR comprises the intracellular domain of mouse FGFR1 fused to the PHR domain from Arabidopsis Cryptochrome 2, which clusters under blue light stimulation. The construct is anchored in the membrane through N-terminal myristoylation. B) Single cell distributions of ppErk intensity in STE-1 cells stimulated by the indicated intensity of blue light in the presence (orange) or absence (grey) of ALKi (2 hr pre-incubation of 1μM crizotinib). Strong ppErk response at low light intensity in the presence, but not the absence, of ALKi suggests that ALKi hypersensitizes cells to RTK stimulation. C) The magnitude of ppErk response in optoFGFR STE-1 cells is a function of both light intensity and optoFGFR expression levels. Results are presented by binning optoFGFR-mCh expression by quartiles. (1<25%, 25% < 2 < 50%, 50% <3 < 75%, 4 > 75%).

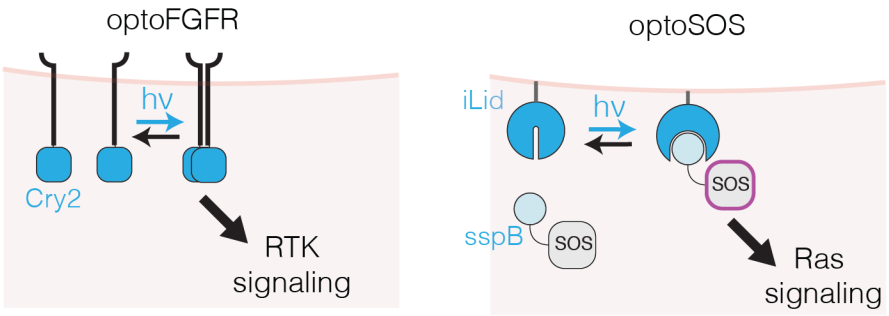

528

529 **Supplementary Figure 2. Schematics of the optoFGFR and optoSOS tools used in Figure**
530 **3.**

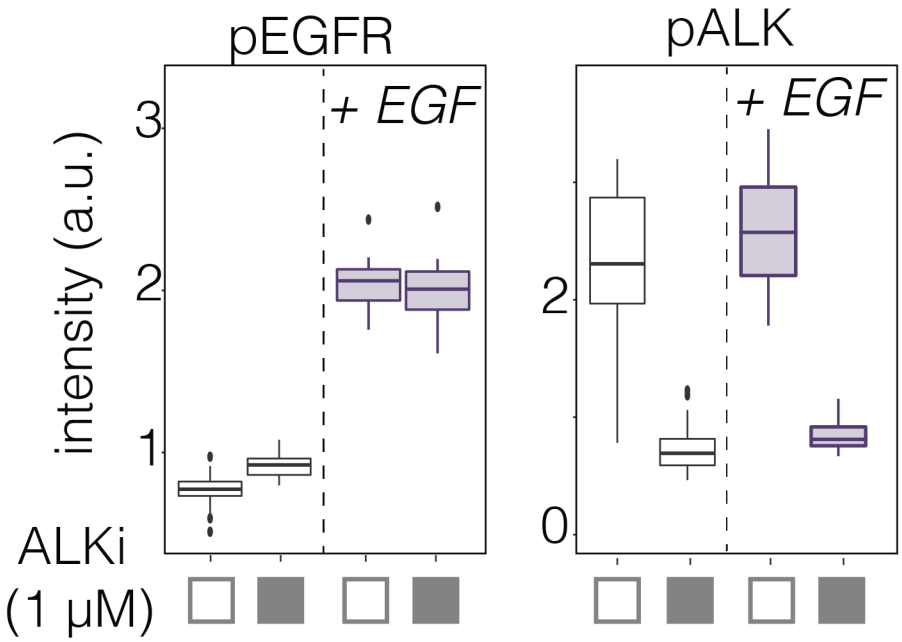

Supplementary Figure 3. EGFR signal suppression does not result from decreased EGFR phosphorylation. Following overnight starvation, STE-1 cells were pretreated with ALKi or DMSO for 2 hrs, were stimulated with either EGF (50 ng/mL) or fresh starvation medium for 15 min, and then were fixed and immunostained. ALKi pretreatment did not alter pEGFR (Y1068) levels in either the presence or absence of EGF, whereas pALK (Y1507) decreased. Thus increased EGFR signaling in ALKi pretreated cells does not result from increased EGFR phosphorylation.

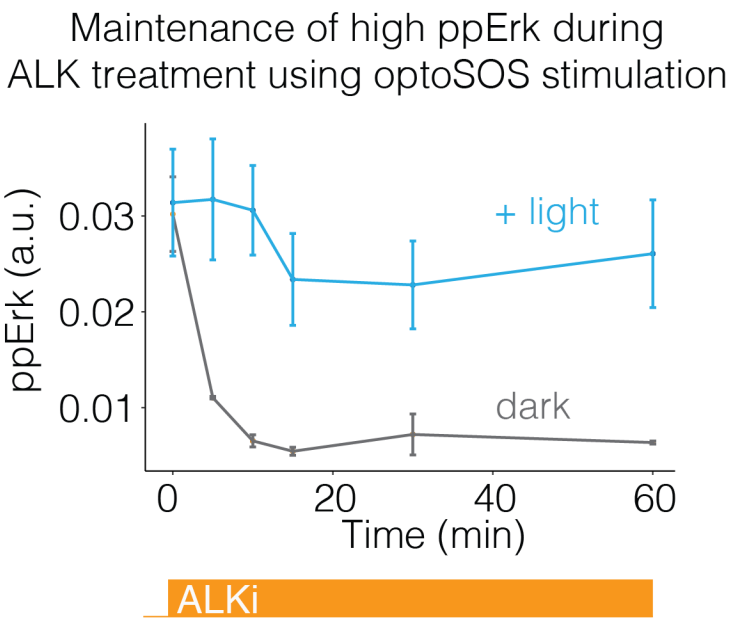

541 **Supplementary Figure 4. Optogenetic maintenance of high ppErk during ALKi treatment.**
542 Demonstration that optoSOS can maintain high Erk levels (comparable to those from the uninhibited
543 oncogene) during ALKi pre-treatment. Optogenetic stimulation of Ras/Erk was used to decouple ALK
544 inhibition from loss of Erk signaling in **Figure 3G-J**.
545

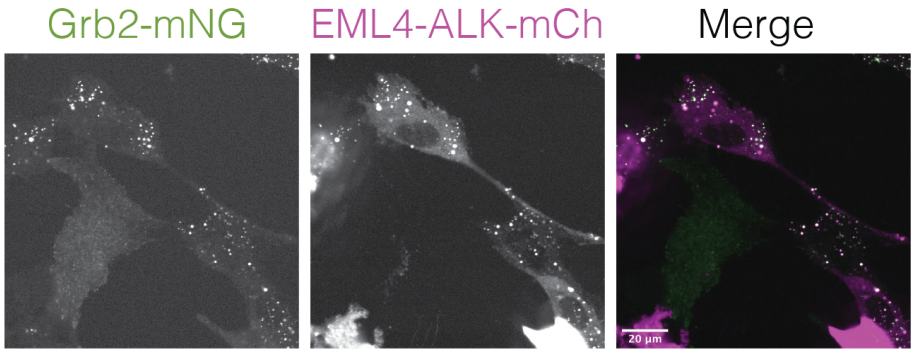

Supplementary Figure 5. EML4-ALK condensates colocalize with Grb2 puncta. Beas2B cells that harbored endogenously tagged Grb2 (Grb2:mNG) were transfected with EML4-ALK-mCh. In transfected cells, EML4-ALK co-localized with Grb2. In untransfected cells, Grb2 was diffuse.

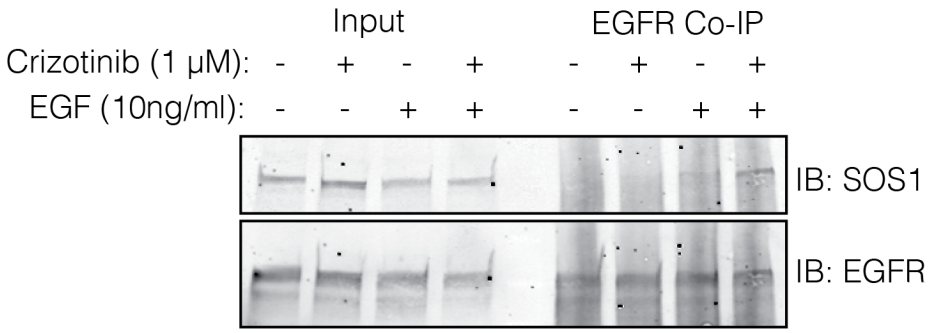

Supplementary Figure 6. Co-immunoprecipitation of EGFR with SOS1. H3122 cells were starved overnight, pretreated with crizotinib (2 hr), and were stimulated with EGF for 2 minutes before lysis and immunoprecipitation. Right 4 lanes are reproduced from **Figure 4J**.

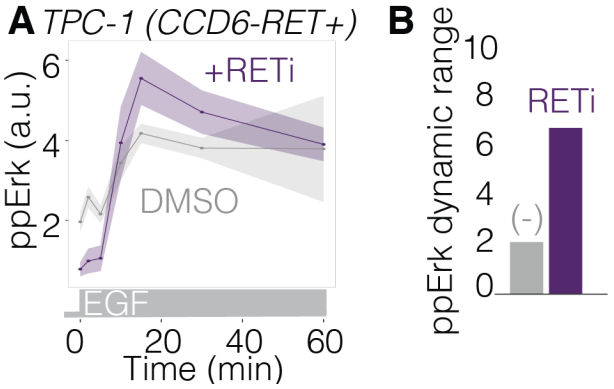

Supplementary Figure 7. CCDC6-RET+ cancer cells show dynamic suppression of EGFR through RTK fusion activity. TPC-1 cells harbor CCDC6-RET, a distinct RTK fusion that forms condensates. We tested the extent to which CCDC6-RET could modulate EGFR dynamic range as observed for EML4-ALK. A) Plot shows ppErk intensity response to EGF stimulation after 2 hr pre-treatment with DMSO (grey) or 1 μM BLU-667 (purple), a RET inhibitor. Data represents mean, and error bars represent 95% CI of triplicates, each of which represents ~1000 cells. B) Quantification of ppErk dynamic range shows that oncogene inhibition enhances signaling through EGFR. Thus, multiple RTK fusions that form condensates dynamically suppress EGFR signaling.

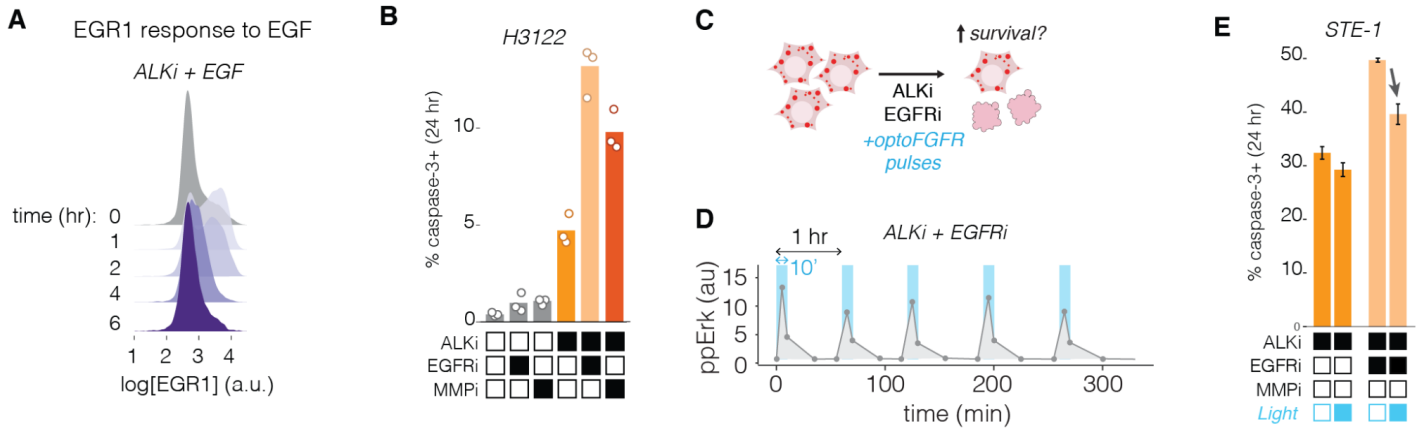

Supplementary Figure 8. RTK/Erk pulses activate transcription and promote cell survival during ALKi treatment. A) Adaptive response of EGR1 expression in STE-1 cells treated with ALKi and 50 ng/mL of EGF. EGR1 peaks at 1 hr after stimulation and then adapts to near baseline expression. EGR response is stronger and earlier than observed in **Figure 6B** because here all cells were stimulated at t = 0, whereas in **6B** only individual cells were stimulated sporadically through paracrine signals starting 1-2 hrs after ALK treatment. B) Blockade of EGFR or MMPs accelerates cell death in H3122 in response to ALKi, as shown STE-1 cells in **Figure 6G**. C) We tested whether optoFGFR stimulation could reduce the enhanced cell death response in STE-1 cells co-treated with ALKi and EGFRi. D). A 10 min pulse of blue light (96 mW/cm^2) every hour produced strong, periodic ppErk levels. E) Hourly pulses of optoFGFR/Erk (10 min of 96 mW/cm^2) reduced cell death in both ALKi and ALKi/EGFRi treated cells. Data represents the mean, error bars = 95% CI caspase-3+ cells of three replicates, each representing ~10,000 cells.

590 **Methods**
591
592 Cell Lines and Cell Culture
593 All cell lines were maintained at 37°C and 5% CO_2 using standard cell culture incubator. STE-1,
594 H3122, TPC-1 and Beas2B cell lines were cultured in RPMI-1640 media containing L-glutamine
595 supplement with 10% fetal bovine serum (FBS) and 1% penicillin/streptomycin (P/S). For
596 experiments, cells were seeded in 96 or 384 well plates coated with 10 µg/mL MilliporeSigma™
597 Chemicon™ Human Plasma Fibronectin Purified Protein in PBS. For 96 well plate experiments
598 10,000 STE-1 and H3122 cells were seeded in 200µl of cell culture media per well. For 384 well
599 plate experiments 5,000 STE-1 cells, 5000 H3122 cells, or 2000 Beas2B cells were seeded in
600 50µl of culture media per well.
601
602 Constructs
603 EML4-ALK variant 1 (EML4ALK(V1)) cDNA was cloned into a pCMV vector with a C-terminal
604 2A-H2B-iRFP670 tag. Deletion of EML4 trimerization domain was achieved by deleting bases
605 310-459 of EML4-ALK full-length sequence GenBank: AB274722.1 and EML4-ALK kinase-dead
606 was cloned by mutating K589M as previously described (Tulpule et al. 2021). EML4ALK(V1)-
607 mCh was cloned by replacing the C-terminal 2A-H2B-iRFP670 tag with mCh. Erk kinase
608 translocation reporter (KTR-mCh) was cloned into a pHR lentiviral vector with a C-terminal mCh
609 tag. H2B-iRFP670 nuclear marker was cloned into a pHR. For optogenetic control of FGFR
610 signaling, the cytoplasmic domain of FGFR1 receptor with an N-terminal myristylation site was
611 fused to the N-terminal of mCh-Cry2. All cloning was performed using NEB Hifi DNA assembly
612 reagent.
613
614 Transfection and viral transduction
615 EML4ALKV1, ΔTD EML4ALK, and K589M EML4ALK plasmids were transfected into Beas2B
616 cells using Lipofectamine™ 3000 Transfection Reagent (Invitrogen, L3000001) following
617 manufacturer recommendations. OptoFGFR, OptoSOS, KTR-mCh, and H2B-iRFP670 vectors
618 were packaged into lentivirus using lentiX- HEK 293T cells. Briefly cells were transfected with
619 pHR packaging vectors and supernatant was collected over two days. 300,000 STE-I cells were
620 then seeded in 6 well plate with media containing virus. Cells were then expanded, and
621 successfully transduced cells were sorted using fluorescence activated cell sorting (BD Influx
622 System)
623
624
625 Optogenetic Stimulation
626 Light stimulation was achieved using a single-color blue LED optoPlate-96(L. J. Bugaj and Lim
627 2019). A 13 mm tall black adaptor was used for even light diffusion across each of the 384 well
628 plate wells being illuminated. Light intensity was corrected to stimulate wells with a range of blue

light intensities spanning from 0 to 870 mW/cm^2. Cells were stimulated for 500ms every 10 seconds at the specified light intensity.

Growth Factor Stimulation Assay

24 hr following cell plating, cells were starved with RPMI-1640 media containing L-glutamine and 1% P/S using the a BioTEK 405 platge washer. 24 hrs after starvation, cells were treated with inhibitor for 2 hours (1μM Crizotinib (Sigma-Aldrich, PZ0191) or 1-100 μM BLU-667 (Biovision, B2548)). Cells were then stimulated at their respective time points with epidermal growth factor (EGF) (PeproTech 315-09) following a delay that allows for all wells to be fixed at the same time. Cells were then immediately prepared for immunostaining.

Immunostaining

Immediately after treatment, cells were fixed using 4% paraformaldehyde for 10 min and permeabilized using 0.5% Triton-X100 in PBS for 10 min. Cells were further permeabilized using 100% methanol at -20°C for 10 min and samples were blocked with 1% bovine serum albumin (Fisher, BP9706100) in PBS (PBS+1%BSA) for 1 hour at room temperature. Cells were then incubated in primary antibody diluted in PBS+1%BSA for 2 hours at room temperature or overnight at 4C (phospho-p44/42 MAPK (Erk1/2) (Thr202/Tyr204), Cell Signaling, catalog number 4370, 1:400 dilution; Phospho-EGF Receptor (Tyr1068), Cell Signaling, catalog number 3777, 1:800; EGR1, Cell Signaling, catalog number 4153, 1:800). Primary antibody was then washed with 0.1% Tween-20 in PBS (PBS+T). Cells were then incubated in secondary antibody diluted in PBS+1%BSA as recommended (IgG (H+L) Cross-Adsorbed Goat anti-Rabbit, DyLight™ 488, Invitrogen, catalog number 35553, 1:500; Goat anti-Rabbit IgG (H+L) Cross-Adsorbed Secondary Antibody, DyLight™ 650, Invitrogen, catalog number SA510034, 1:500) and and 4,6-diamidino-2-phenylindole (DAPI; ThermoFisher Scientific, catalog number D1306, 300 nM) for 1 hour at room temperature and washed with PBS+T.

Live Cell Imaging

A Nikon Ti2-E microscope equipped with a Yokagawa CSU-W1 spinning disk, 405/488/561/640 nm laser lines, an sCMOS camera (Photometrics), and a motorized stage was used for live cell imaging. Temperature was maintained at 37°C and CO2 concentration was maintained at 5% using an environmental chamber (Okolabs). Transfected Beas2B::mNGGrb2 cells were imaged 48 hours after transfection with a 40X oil immersion lens. To visualize Grb2 localization in response to growth factor stimulation after oncogene inhibition, cells were imaged for 2 hours following 1μM crizotinib treatment. Cells were then stimulated with 50 ng/mL EGF (PreproTech 315-09). STE1 cells stably expressing ERKKTR-Ruby and H2B-iRFP670 were seeded in a 96 well plate (1.5x10^5 cells/well) and cultured in RPMI supplemented with 2% FBS. 48 hours post-seeding, cells were supplemented with NucView (1:1000), Criztinib (1 μM), Erlotinib (1 μM), Marimastat (10 μM) or DMSO (1:5000). Cells were imaged every 5 minutes for 22 hours at 20X magnification.

669
670 Cell Death Assay
671 The day following cell plating, cells were washed with phenol free RPMI-1640 with L-glutamine
672 supplemented with 2% FBS, 1% P/S, 1μM NucView 488, and respective inhibitor treatment
673 (Crizotinib 1μM, Erlotinib 1μM, Marimastat 10μM). 24 hours after treatment addition, cells were
674 treated with 5 μg/mL Hoechst 33342 Hydrochloride (Cayman 15547) for 15 minutes. Cells were
675 then imaged using confocal microscopy as previously described.
676
677 Image Processing and Analysis
678 Immunostaining and live imaging of caspase+ cells was performed using Cell Profiler version
679 4.0.7. Briefly, cell nuclei were segmented using the DAPI or Hoechst 33342 Hydrochloride stain
680 and cytoplasm was obtained by expanding a 5-pixel ring from the nuclei. Data was then exported
681 into R for data visualization using the dplyr and ggplot2 packages.
682
683 Live cell image analysis.
684 *Grb2 cluster dissociation*
685 Grb2 clusters time lapse imaging was quantified with a custom MATLAB script. Briefly, cells
686 were segmented manually and clusters were identified through the following steps. First, cell
687 intensities were first normalized to their internal median, and a series of transforms were
688 performed to enhance clusters while suppressing other features, like background and high
689 frequency noise. These transformed intensities were used to identify bright pixels at the center
690 of clusters, using a user-defined intensity cutoff. From each of these center points, neighboring
691 pixels were compared to a threshold intensity that was set by the local background of the cell
692 and scaled by a second user-defined parameter. Neighboring pixels above this threshold are
693 included in the cluster, while pixels below the threshold are excluded. This occurs iteratively,
694 where adjacent pixels to each included pixel were also checked to be included or excluded
695 until all new neighbors were below the threshold.
696
697
698 *ErkKTR dynamics*
699 ErkKTR dynamics and cell death were tracked and quantitated in a semi-automated manner
700 using the p53CellCinema package (Reyes et al. 2018) in MATLAB, and data was processed and
701 visualized in R and RStudio using the tidyR(Wickham et al. 2019) package. Briefly, cells with
702 low or no ErkKTR expression were first excluded from analysis. Then, ErkKTR
703 cytoplasmic/nuclear ratios from remaining cells were imported into MATLAB, and peaks were
704 identified using the 'findpeaks' function. Peak calls were then manually inspected for outliers, for
705 example resulting from apoptotic cell debris, and outlier cells were removed from analysis. Of
706 note, we consistently observed Erk pulses preceding cell division events across conditions. This
707 phenomenon has been previously observed and has been shown to be independent of Ras/Erk
708 signaling, potentially due to non-specific activation from a cyclin dependent kinase(Gerosa et al.

2020). Thus, we disregarded all pulses that occurred within 10 frames (50 mins) preceding cell division. To count Erk pulses in neighbors vs non-neighbors of dying cells, we first identified each cell death event. We then identified the neighbors of the dying cell by identifying which nuclei centroids were within a 100 pixel radius of the dying cell for each of the 10 frames preceding the death annotation. We then counted the total pulses of those neighbors over the indicated time frame, and compared against pulse counts from a random subset of non-neighbor cells over the same time frame. Importantly, for each death event, the number of non-neighbors that were sampled matched the number of neighbors, and the sampled non-neighbors were not neighbors of other death events over that same time span. For visualization in **Figure 6E**, cells that divided during the course of the experiment are represented as separate cells, and the Erk history of the mother cell is reproduced for both cells. However, for quantification of Erk pulses, mother cell pulses were counted only once.

References

Banani, Salman F., Hyun O. Lee, Anthony A. Hyman, and Michael K. Rosen. 2017. "Biomolecular Condensates: Organizers of Cellular Biochemistry." *Nature Reviews. Molecular Cell Biology* 18 (5): 285–98.

Benman, William, Erin E. Berlew, Hao Deng, Caitlyn Parker, Ivan A. Kuznetsov, Bomyi Lim, Arndt F. Siekmann, Brian Y. Chow, and Lukasz J. Bugaj. 2022. "Temperature-Responsive Optogenetic Probes of Cell Signaling." *Nature Chemical Biology* 18 (2): 152–60.

Brachmann, R., P. B. Lindquist, M. Nagashima, W. Kohr, T. Lipari, M. Napier, and R. Derynck. 1989. "Transmembrane TGF-Alpha Precursors Activate EGF/TGF-Alpha Receptors." *Cell* 56 (4): 691–700.

Bugaj, L. J., A. J. Sabnis, A. Mitchell, J. E. Garbarino, J. E. Toettcher, T. G. Bivona, and W. A. Lim. 2018. "Cancer Mutations and Targeted Drugs Can Disrupt Dynamic Signal Encoding by the Ras-Erk Pathway." *Science* 361 (6405). https://doi.org/10.1126/science.aao3048.

Bugaj, Lukasz J., Geoff P. O'Donoghue, and Wendell A. Lim. 2017. "Interrogating Cellular Perception and Decision Making with Optogenetic Tools." *The Journal of Cell Biology* 216 (1): 25–28.

Cai, Danfeng, Zhe Liu, and Jennifer Lippincott-Schwartz. 2021. "Biomolecular Condensates and Their Links to Cancer Progression." *Trends in Biochemical Sciences* 46 (7): 535–49.

Corcoran, Ryan B., Hiromichi Ebi, Alexa B. Turke, Erin M. Coffee, Michiya Nishino, Alexandria P. Cogdill, Ronald D. Brown, et al. 2012. "EGFR-Mediated Re-Activation of MAPK Signaling Contributes to Insensitivity of BRAF Mutant Colorectal Cancers to RAF Inhibition with Vemurafenib." *Cancer Discovery* 2 (3): 227–35.

Davies, Kurtis D., Sakshi Mahale, David P. Astling, Dara L. Aisner, Anh T. Le, Trista K. Hinz, Aria Vaishnavi, et al. 2013. "Resistance to ROS1 Inhibition Mediated by EGFR Pathway Activation in Non-Small Cell Lung Cancer." *PloS One* 8 (12): e82236.

Dong, J., L. K. Opresko, P. J. Dempsey, D. A. Lauffenburger, R. J. Coffey, and H. S. Wiley. 1999. "Metalloprotease-Mediated Ligand Release Regulates Autocrine Signaling through the Epidermal Growth Factor Receptor." *Proceedings of the National Academy of Sciences of the*

755 *United States of America* 96 (11): 6235–40.
756 Du, Zhenfang, and Christine M. Lovly. 2018. “Mechanisms of Receptor Tyrosine Kinase Activation in
757 Cancer.” *Molecular Cancer* 17 (1): 58.
758 Gagliardi, Paolo Armando, Maciej Dobrzyński, Marc-Antoine Jacques, Coralie Dessauges, Pascal
759 Ender, Yannick Blum, Robert M. Hughes, Andrew R. Cohen, and Olivier Pertz. 2021. “Collective
760 ERK/Akt Activity Waves Orchestrate Epithelial Homeostasis by Driving Apoptosis-Induced
761 Survival.” *Developmental Cell* 56 (12): 1712-1726.e6.
762 Gainor, Justin F., Leila Dardaei, Satoshi Yoda, Luc Friboulet, Ignaty Leshchiner, Ryohei Katayama,
763 Ibiayi Dagogo-Jack, et al. 2016. “Molecular Mechanisms of Resistance to First- and Second-
764 Generation ALK Inhibitors in ALK-Rearranged Lung Cancer.” *Cancer Discovery* 6 (10): 1118–
765 33.
766 Garabedian, Mikael V., Wentao Wang, Jorge B. Dabdoub, Michelle Tong, Reese M. Caldwell, William
767 Benman, Benjamin S. Schuster, Alexander Deiters, and Matthew C. Good. 2021. “Designer
768 Membraneless Organelles Sequester Native Factors for Control of Cell Behavior.” *Nature*
769 *Chemical Biology* 17 (9): 998–1007.
770 Gerosa, Luca, Christopher Chidley, Fabian Fröhlich, Gabriela Sanchez, Sang Kyun Lim, Jeremy
771 Muhlich, Jia-Yun Chen, et al. 2020a. “Receptor-Driven ERK Pulses Reconfigure MAPK
772 Signaling and Enable Persistence of Drug-Adapted BRAF-Mutant Melanoma Cells.” *Cell*
773 *Systems* 11 (5): 478-494.e9.
774 Hirai, Noriko, Takaaki Sasaki, Shunsuke Okumura, Yoshinori Minami, Shinichi Chiba, and Yoshinobu
775 Ohsaki. 2020. “Monomerization of ALK Fusion Proteins as a Therapeutic Strategy in ALK-
776 Rearranged Non-Small Cell Lung Cancers.” *Frontiers in Oncology* 10 (April): 419.
777 Hrustanovic, Gorjan, Victor Olivas, Evangelos Pazarentzos, Asmin Tulpule, Saurabh Asthana, Collin M.
778 Blakely, Ross A. Okimoto, et al. 2015. “RAS-MAPK Dependence Underlies a Rational
779 Polytherapy Strategy in EML4-ALK–Positive Lung Cancer.” *Nature Medicine* 21 (August): 1038.
780 Jiang, Shan, Johan Bourghardt Fagman, Changyan Chen, Simon Alberti, and Beidong Liu. 2020.
781 “Protein Phase Separation and Its Role in Tumorigenesis.” *ELife* 9 (November).
782 https://doi.org/10.7554/eLife.60264.
783 Kim, Nury, Jin Man Kim, Minji Lee, Cha Yeon Kim, Ki-Young Chang, and Won Do Heo. 2014.
784 “Spatiotemporal Control of Fibroblast Growth Factor Receptor Signals by Blue Light.” *Chemistry*
785 *& Biology* 21 (7): 903–12.
786 Kurtova, Antonina V., Jing Xiao, Qianxing Mo, Senthil Pazhanisamy, Ross Krasnow, Seth P. Lerner,
787 Fengju Chen, et al. 2015. “Blocking PGE2-Induced Tumour Repopulation Abrogates Bladder
788 Cancer Chemoresistance.” *Nature* 517 (7533): 209–13.
789 Lito, Piro, Christine A. Pratilas, Eric W. Joseph, Madhavi Tadi, Ensar Halilovic, Matthew Zubrowski,
790 Alan Huang, et al. 2012a. “Relief of Profound Feedback Inhibition of Mitogenic Signaling by RAF
791 Inhibitors Attenuates Their Activity in BRAFV600E Melanomas.” *Cancer Cell* 22 (5): 668–82.
792 Lovly, Christine M., Nerina T. McDonald, Heidi Chen, Sandra Ortiz-Cuaran, Lukas C. Heukamp,
793 Yingjun Yan, Alexandra Florin, et al. 2014. “Rationale for Co-Targeting IGF-1R and ALK in ALK
794 Fusion-Positive Lung Cancer.” *Nature Medicine* 20 (9): 1027–34.
795 Miller, Miles A., Madeleine J. Oudin, Ryan J. Sullivan, Stephanie J. Wang, Aaron S. Meyer, Hyungsoon
796 Im, Dennie T. Frederick, et al. 2016. “Reduced Proteolytic Shedding of Receptor Tyrosine
797 Kinases Is a Post-Translational Mechanism of Kinase Inhibitor Resistance.” *Cancer Discovery* 6
798 (4): 382–99.
799 Obenauf, Anna C., Yilong Zou, Andrew L. Ji, Sakari Vanharanta, Weiping Shu, Hubing Shi, Xiangju
800 Kong, et al. 2015. “Therapy-Induced Tumour Secretomes Promote Resistance and Tumour
801 Progression.” *Nature* 520 (7547): 368–72.
802 Omer, Amr, Devang Patel, Xian Jin Lian, Jason Sadek, Sergio Di Marco, Arnim Pause, Myriam
803 Gorospe, and Imed Eddine Gallouzi. 2018. “Stress Granules Counteract Senescence by
804 Sequestration of PAI-1.” *EMBO Reports* 19 (5). https://doi.org/10.15252/embr.201744722.
805 Ou, Sai-Hong Ignatius, Ramaswamy Govindan, Keith D. Eaton, Gregory A. Otterson, Martin E.

806 Gutierrez, Alain C. Mita, Athanassios Argiris, et al. 2017. “Phase I Results from a Study of
807 Crizotinib in Combination with Erlotinib in Patients with Advanced Nonsquamous Non-Small Cell
808 Lung Cancer.” *Journal of Thoracic Oncology: Official Publication of the International Association*
809 *for the Study of Lung Cancer* 12 (1): 145–51.
810 Peschon, J. J., J. L. Slack, P. Reddy, K. L. Stocking, S. W. Sunnarborg, D. C. Lee, W. E. Russell, et al.
811 1998. “An Essential Role for Ectodomain Shedding in Mammalian Development.” *Science* 282
812 (5392): 1281–84.
813 Prahallad, Anirudh, Chong Sun, Sidong Huang, Federica Di Nicolantonio, Ramon Salazar, Davide
814 Zecchin, Roderick L. Beijersbergen, Alberto Bardelli, and René Bernards. 2012a.
815 “Unresponsiveness of Colon Cancer to BRAF(V600E) Inhibition through Feedback Activation of
816 EGFR.” *Nature* 483 (7387): 100–103.
817 Regot, Sergi, Jacob J. Hughey, Bryce T. Bajar, Silvia Carrasco, and Markus W. Covert. 2014. “High-
818 Sensitivity Measurements of Multiple Kinase Activities in Live Single Cells.” *Cell* 157 (7): 1724–
819 34.
820 Rusch, V., J. Baselga, C. Cordon-Cardo, J. Orazem, M. Zaman, S. Hoda, J. McIntosh, J. Kurie, and E.
821 Dmitrovsky. 1993. “Differential Expression of the Epidermal Growth Factor Receptor and Its
822 Ligands in Primary Non-Small Cell Lung Cancers and Adjacent Benign Lung.” *Cancer Research*
823 53 (10 Suppl): 2379–85.
824 Sahin, Umut, Gisela Weskamp, Kristine Kelly, Hong-Ming Zhou, Shigeki Higashiyama, Jacques
825 Peschon, Dieter Hartmann, Paul Saftig, and Carl P. Blobel. 2004. “Distinct Roles for ADAM10
826 and ADAM17 in Ectodomain Shedding of Six EGFR Ligands.” *The Journal of Cell Biology* 164
827 (5): 769–79.
828 Sampson, Josephina, Mark W. Richards, Jene Choi, Andrew M. Fry, and Richard Bayliss. 2021.
829 “Phase-Separated Foci of EML4-ALK Facilitate Signalling and Depend upon an Active Kinase
830 Conformation.” *EMBO Reports*, October, e53693.
831 Sasaki, Takaaki, Jussi Koivunen, Atsuko Ogino, Masahiko Yanagita, Sarah Nikiforow, Wei Zheng,
832 Christopher Lathan, et al. 2011. “A Novel ALK Secondary Mutation and EGFR Signaling Cause
833 Resistance to ALK Kinase Inhibitors.” *Cancer Research* 71 (18): 6051–60.
834 Shaw, Alice T., Peggy P. Hsu, Mark M. Awad, and Jeffrey A. Engelman. 2013. “Tyrosine Kinase Gene
835 Rearrangements in Epithelial Malignancies.” *Nature Reviews. Cancer* 13 (11): 772–87.
836 Siegel, Rebecca L., Kimberly D. Miller, Hannah E. Fuchs, and Ahmedin Jemal. 2021. “Cancer
837 Statistics, 2021.” *CA: A Cancer Journal for Clinicians* 71 (1): 7–33.
838 Solomon, Benjamin J., Benjamin Besse, Todd M. Bauer, Enriqueta Felip, Ross A. Soo, D. Ross
839 Camidge, Rita Chiari, et al. 2018. “Lorlatinib in Patients with ALK-Positive Non-Small-Cell Lung
840 Cancer: Results from a Global Phase 2 Study.” *The Lancet Oncology* 19 (12): 1654–67.
841 Straussman, Ravid, Teppei Morikawa, Kevin Shee, Michal Barzily-Rokni, Zhi Rong Qian, Jinyan Du,
842 Ashli Davis, et al. 2012. “Tumour Micro-Environment Elicits Innate Resistance to RAF Inhibitors
843 through HGF Secretion.” *Nature* 487 (7408): 500–504.
844 Sukhatme, V. P., S. Kartha, F. G. Toback, R. Taub, R. G. Hoover, and C. H. Tsai-Morris. 1987. “A
845 Novel Early Growth Response Gene Rapidly Induced by Fibroblast, Epithelial Cell and
846 Lymphocyte Mitogens.” *Oncogene Research* 1 (4): 343–55.
847 Takeuchi, Kengo, Manabu Soda, Yuki Togashi, Ritsuro Suzuki, Seiji Sakata, Satoko Hatano, Reimi
848 Asaka, et al. 2012. “RET, ROS1 and ALK Fusions in Lung Cancer.” *Nature Medicine* 18 (3):
849 378–81.
850 Tani, Tetsuo, Hiroyuki Yasuda, Junko Hamamoto, Aoi Kuroda, Daisuke Arai, Kota Ishioka, Keiko
851 Ohgino, et al. 2016. “Activation of EGFR Bypass Signaling by TGFα Overexpression Induces
852 Acquired Resistance to Alectinib in ALK-Translocated Lung Cancer Cells.” *Molecular Cancer*
853 *Therapeutics* 15 (1): 162–71.
854 Tanimoto, Azusa, Tadaaki Yamada, Shigeki Nanjo, Shinji Takeuchi, Hiromichi Ebi, Kenji Kita, Kunio
855 Matsumoto, and Seiji Yano. 2014. “Receptor Ligand-Triggered Resistance to Alectinib and Its
856 Circumvention by Hsp90 Inhibition in EML4-ALK Lung Cancer Cells.” *Oncotarget* 5 (13): 4920–

857 28.
858 Thedieck, Kathrin, Birgit Holzwarth, Mirja Tamara Prentzell, Christopher Boehlke, Kathrin Kläsener,
859 Stefanie Ruf, Annika Gwendolin Sonntag, et al. 2013. “Inhibition of MTORC1 by Astrin and
860 Stress Granules Prevents Apoptosis in Cancer Cells.” *Cell* 154 (4): 859–74.
861 Toettcher, J. E., O. D. Weiner, and W. A. Lim. 2013. “Using Optogenetics to Interrogate the Dynamic
862 Control of Signal Transmission by the Ras/Erk Module.” *Cell* 155 (6): 1422–34.
863 Tulpule, Asmin, Juan Guan, Dana S. Neel, Hannah R. Allegakoen, Yone Phar Lin, David Brown, Yu-
864 Ting Chou, et al. 2021. “Kinase-Mediated RAS Signaling via Membraneless Cytoplasmic Protein
865 Granules.” *Cell*, April. https://doi.org/10.1016/j.cell.2021.03.031.
866 Turke, Alexa B., Youngchul Song, Carlotta Costa, Rebecca Cook, Carlos L. Arteaga, John M. Asara,
867 and Jeffrey A. Engelman. 2012. “MEK Inhibition Leads to PI3K/AKT Activation by Relieving a
868 Negative Feedback on ERBB Receptors.” *Cancer Research* 72 (13): 3228–37.
869 Vaishnavi, Aria, Laura Schubert, Uwe Rix, Lindsay A. Marek, Anh T. Le, Stephen B. Keysar,
870 Magdalena J. Glogowska, et al. 2017. “EGFR Mediates Responses to Small-Molecule Drugs
871 Targeting Oncogenic Fusion Kinases.” *Cancer Research* 77 (13): 3551–63.
872 Vander Velde, Robert, Nara Yoon, Viktoriya Marusyk, Arda Durmaz, Andrew Dhawan, Daria
873 Miroshnychenko, Diego Lozano-Peral, et al. 2020. “Resistance to Targeted Therapies as a
874 Multifactorial, Gradual Adaptation to Inhibitor Specific Selective Pressures.” *Nature*
875 *Communications* 11 (1): 2393.
876 Voena, C., F. Di Giacomo, E. Panizza, L. D’Amico, F. E. Boccalatte, E. Pellegrino, M. Todaro, et al.
877 2013. “The EGFR Family Members Sustain the Neoplastic Phenotype of ALK+ Lung
878 Adenocarcinoma via EGR1.” *Oncogenesis* 2 (April): e43.
879 Weinstein, I. Bernard. 2002. “Cancer. Addiction to Oncogenes--the Achilles Heal of Cancer.” *Science*.
880 Wilson, Maxwell Z., Pavithran T. Ravindran, Wendell A. Lim, and Jared E. Toettcher. 2017. “Tracing
881 Information Flow from Erk to Target Gene Induction Reveals Mechanisms of Dynamic and
882 Combinatorial Control.” *Molecular Cell* 67 (5): 757-769.e5.
883 Wilson, Timothy R., Jane Fridlyand, Yibing Yan, Elicia Penuel, Luciana Burton, Emily Chan, Jing Peng,
884 et al. 2012. “Widespread Potential for Growth-Factor-Driven Resistance to Anticancer Kinase
885 Inhibitors.” *Nature* 487 (7408): 505–9.
886 Wong, S. T., L. F. Winchell, B. K. McCune, H. S. Earp, J. Teixidó, J. Massagué, B. Herman, and D. C.
887 Lee. 1989. “The TGF-Alpha Precursor Expressed on the Cell Surface Binds to the EGF
888 Receptor on Adjacent Cells, Leading to Signal Transduction.” *Cell* 56 (3): 495–506.